NeuroImage: Clinical 17 (2018) 198–212

Contents lists available at ScienceDirect

NeuroImage: Clinical

journal homepage: www.elsevier.com/locate/ynicl

Reorganization of the somatosensory cortex in hemiplegic cerebral palsy associated with impaired sensory tracts

Christos Papadelis[a,b,*], Erin E. Butler[c,d], Madelyn Rubenstein[a,b], Limin Sun[a,b], Lilla Zollei[e], Donna Nimec[f], Brian Snyder[f], Patricia Ellen Grant[a,b,g]

[a] Fetal-Neonatal Neuroimaging & Developmental Science Center, Boston Children's Hospital, Harvard Medical School, Boston, MA, USA
[b] Division of Newborn Medicine, Department of Medicine, Boston Children's Hospital, Harvard Medical School, Boston, MA, USA
[c] Thayer School of Engineering, Dartmouth College, Hanover, NH, USA
[d] William H. Neukom Institute for Computational Science, Dartmouth College, Hanover, NH, USA
[e] Athinoula A. Martinos Center for Biomedical Imaging, Massachusetts General Hospital, Harvard Medical School, Charlestown, MA, USA
[f] Department of Orthopedic Surgery, Boston Children's Hospital, Harvard Medical School, Boston, MA, USA
[g] Department of Radiology, Boston Children's Hospital, Harvard Medical School, Boston, MA, USA

ARTICLE INFO

Keywords:
Brain injury
Brain reorganization
Hemiplegic cerebral palsy
Cortical plasticity
Hemiplegia
Magnetoencephalography
Probabilistic diffusion tractography
Somatosensory deficits

ABSTRACT

Functional neuroimaging studies argue that sensory deficits in hemiplegic cerebral palsy (HCP) are related to deviant somatosensory processing in the ipsilesional primary somatosensory cortex (S1). A separate body of structural neuroimaging literature argues that these deficits are due to structural damage of the ascending sensory tracts (AST). The relationship between the functional and structural integrity of the somatosensory system and the sensory performance is largely unknown in HCP. To address this relationship, we combined findings from magnetoencephalography (MEG) and probabilistic diffusion tractography (PDT) in 10 children with HCP and 13 typically developing (TD) children. With MEG, we mapped the functionally active regions in the contralateral S1 during tactile stimulation of the thumb, middle, and little fingers of both hands. Using these MEG-defined functional active regions as regions of interest for PDT, we estimated the diffusion parameters of the AST. Somatosensory function was assessed via two-point discrimination tests. Our MEG data showed: (i) an abnormal somatotopic organization in all children with HCP in either one or both of their hemispheres; (ii) longer Euclidean distances between the digit maps in the S1 of children with HCP compared to TD children; (iii) suppressed gamma responses at early latencies for both hemispheres of children with HCP; and (iv) a positive correlation between the Euclidean distances and the sensory tests for the more affected hemisphere of children with HCP. Our MEG-guided PDT data showed: (i) higher mean and radian diffusivity of the AST in children with HCP; (ii) a positive correlation between the axial diffusivity of the AST with the sensory tests for the more affected hemisphere; and (iii) a negative correlation between the gamma power change and the AD of the AST for the MA hemisphere. Our findings associate for the first time bilateral cortical functional reorganization in the S1 of HCP children with abnormalities in the structural integrity of the AST, and correlate these abnormalities with behaviorally-assessed sensory deficits.

1. Introduction

Cerebral palsy (CP) is defined as a group of non-progressive disorders of movement and posture due to a defect or lesion in the developing brain (Rosenbaum et al., 2007). The most common form of CP is hemiplegic CP (HCP) that impairs the use of one hand and disrupts bimanual co-ordination. More than 95% of children with CP suffer from sensory deficits in their upper extremities, such as limited proprioception, stereognosis, and tactile discrimination (Lesný et al., 1993; Sanger and Kukke, 2007; Wingert et al., 2008; Riquelme and Montoya, 2010). The neurophysiological mechanisms underlying these sensory deficits remain unclear. Yet, it has been proposed that abnormal and limited movements of CP contribute to repetitive, aberrant sensory inputs to the immature brain, resulting in abnormal sensory feedback and altered cortical organization (Coq et al., 2008). The development of fine motor skills depends heavily on the somatosensory system (Cascio, 2010), and tactile feedback from mechanoreceptors in the skin and joints is critical to the online modulation of fine motor skills, such as the pinch grip (Soechting and Flanders, 2008; Papadelis et al., 2016). Therefore, it is not surprising that motor dysfunction in children with CP strongly

* Corresponding author at: Boston Children's Hospital, Harvard Medical School, 300 Longwood Ave, Boston, MA 02115, USA.
E-mail address: christos.papadelis@childrens.harvard.edu (C. Papadelis).

http://dx.doi.org/10.1016/j.nicl.2017.10.021
Received 26 April 2017; Received in revised form 27 September 2017; Accepted 18 October 2017
Available online 19 October 2017

correlates with somatosensory impairments (Kinnucan et al., 2010; Auld et al., 2012).

Converging evidence from neurophysiological, behavioral, and functional neuroimaging studies supports altered somatosensory processing in the brains of children with CP. Electroencephalography (EEG) and magnetoencephalography (MEG) studies of CP have reported abnormal amplitude, latency, morphology, and/or somatotopy of cortical somatosensory evoked potentials or fields. These were in response to electrical stimulation of the median nerve, tibial nerve, or tactile stimulation of the hand digits (Wilke and Staudt, 2009; Teflioudi et al., 2011; Kurz and Wilson, 2011; Guo et al., 2012; Nevalainen et al., 2012; Papadelis et al., 2014). Furthermore, the magnitude of the somatosensory cortical activity was found to be related to the mobility and strength impairments seen in children with CP (Kurz et al., 2015b). Few previous MEG studies also reported changes in the oscillatory activity of CP in response to the application of peripheral somatosensations (Guo et al., 2012; Pihko et al., 2014; Kurz et al., 2014, 2015a, 2015b; Becker, et al. 2015). Except Guo et al. (2012) and Kurz et al. (2017), these studies focused their attention on lower frequency bands (i.e., alpha and beta), which are traditionally considered to be closely tied to the activation of the sensory cortex (van Ede et al., 2011). Nevertheless, frequencies in the gamma band are of particular importance since they are more spatially discrete and somatotopically specific than lower frequency oscillations (Crone et al., 1998). Synchronization in gamma frequencies might characterize ‘skillful’ cortical representations, as for example, the thumb representation in the primary somatosensory cortex (S1) (Tecchio et al., 2003). Gamma activity in the S1 has been previously reported in the brain of healthy adults after the delivery of painful (Gross et al., 2007) and non-painful somatosensory stimuli (Tecchio et al., 2003, 2008; Bauer et al., 2006; Fukuda et al., 2008; Witzel et al., 2011). In a recent work by Kurz and colleagues (2017), MEG cortical oscillations, between 10 and 75 Hz, in response to paired-pulse electrical stimulation of the tibial nerve were found to be weaker in children with CP compared to TD children. Our previous MEG study (Papadelis et al., 2014) revealed evidence of functional reorganization in the S1 of children with CP; S1 cortical activations in response to tactile stimulation of the first, third and fifth digits were farther apart in children with CP than in typically developing (TD) children. Functional abnormalities observed in the event-related potentials, evoked by tactile stimulation of the hands, have been further correlated with deficits in two-point discrimination as assessed by neurobehavioral tests (Maitre et al., 2012). In line with these findings, smaller response magnitudes and constricted spatial extents were observed with functional magnetic resonance imaging (fMRI) in the primary and secondary somatosensory cortexes of individuals with mild spastic CP compared to TD individuals during tactile stimulation of the hands (Wingert et al., 2010). Resting-state fMRI studies also showed abnormalities in the functionally connected networks in the somatosensory cortex of individuals with CP (Burton et al., 2009; Papadelis et al., 2014). Altogether, these functional neuroimaging studies suggest a direct association between abnormalities in the somatosensory cortex and diminished somatosensory function in CP.

Altered somatosensory function may not be due to abnormalities in the somatosensory cortex alone. In fact, a growing body of evidence from diffusion tensor imaging (DTI) and tractography studies has demonstrated that the ascending thalamocortical tracts (AST) have more influence on the motor and somatosensory function than the corticospinal motor tracts in CP (Hoon et al., 2002, 2009; Thomas et al., 2005; Trivedi et al., 2010; Rose et al., 2011; Tsao et al., 2015). Hoon et al. (2002, 2009) demonstrated that the severity of injury in the AST was directly linked to deficits in the sensorimotor function, while injury to the corticospinal tracts did not relate to measures of strength or sensation. Reduced fractional anisotropy, reduced tract volume, and increased mean diffusivity of the thalamocortical projections were also reported in the ipsilesional hemisphere of children with congenital hemiplegia (Tsao et al., 2015). The aforementioned findings from anatomical neuroimaging studies indicate that the behaviorally-observed sensory deficits in children with CP – and possibly the functional abnormalities seen with functional neuroimaging in the somatosensory system – could be due to damage to the AST. However, a direct link between the anatomical and functional findings is still missing, possibly because the same individuals with CP are rarely examined with multimodal neuroimaging. Such an attempt to integrate findings from different neuroimaging techniques that assess the structural and functional aspects of the somatosensory system was made in our previous multimodal neuroimaging study (Papadelis et al., 2014). Preliminary data from a small cohort of children with CP were presented showing evidence of abnormal functionality in the S1 and damaged thalamocortical pathways in the more affected (MA) hemisphere of children with CP. However, the cohort of patients was inhomogeneous consisting of both diplegic and hemiplegic patients with CP. More importantly, the neuroimaging findings from the different techniques were evaluated in isolation.

In the current study, we aim to integrate functional and structural lines of evidence to assess the integrity of the somatosensory system in the same cohort of children with HCP. Our main hypothesis is that functional somatosensory deficits in children with HCP are related to abnormal functional processing in the ipsilesional S1 as a result of damaged AST. Based on preliminary data from our previous study (Papadelis et al., 2014), we specifically hypothesize that somatosensory magnetic fields elicited by the tactile stimulation of the hand digits will present abnormal amplitude, latency, oscillatory activity, and somatotopy in the MA hemisphere of children with HCP. These functional abnormalities will be correlated to the severity of damage in the AST and to the behaviorally-assessed sensory deficits. To test our hypothesis, we integrate findings from MEG and probabilistic diffusion tractography (PDT) using a MEG-guided tractography technique. Unlike traditional anatomy-based DTI methods, this approach does not make assumptions about structure-function relationships that may not hold after cortical reorganization (Reid et al., 2016). It is thus expected to provide new information on the altered structure-function relationships arising during brain development in children with HCP. By using this approach, we provide here a direct association of measures of functional cortical organization in the S1 of HCP children with measures of structural integrity of the AST and measures of the severity of sensory deficits.

2. Material and methods

2.1. Participants

Neuroimaging data were assessed from 10 children with spastic HCP (age = 12.3 ± 3.9 years; 4 females) and 13 age-matched TD children (age = 12.5 ± 3.5 years; 8 females). The clinical characteristics of participants with HCP are shown in Table 1. Inclusion criteria were: (i) Gross Motor Function Classification System (GMFCS) level I or II (Palisano et al., 1997), (ii) Manual Abilities Classification Scale (MACS) I or II (Eliasson et al., 2006), (iii) asymmetrical motor impairment assessed by a physiatrist (D.N.), and (iv) ability to follow verbal instructions. Exclusion criteria were: (i) metallic implants, devices, or pumps, (ii) history of brain operation, or (iii) any genetic syndrome or severe intellectual developmental disability. The TD children were right-handed and had no history of neurological disorder or brain injury. Handedness in children with HCP was determined based on the higher functioning hand. The Institutional Review Board at Boston Children's Hospital reviewed and approved this investigation. Informed consent was acquired from the parents and the children assented to participate in the study.

2.2. Somatosensory testing

Touch sensitivity was measured at the tip of the thumb (D1), middle

Table 1
Patient demographics and MRI findings.

ID	Sex	Age	GA (weeks)	Epilepsy	Medications	GMFCS	MACS	MA hemisphere	Lesion type	Lesion size	Lesion location		Lesion extension	
											Th	PW	IC	BS
HCP1	M	6	27	No	–	2	1	Right	PV-WMI	1	–	+	–	–
HCP2	F	15	Term	No	–	1	1	Right	PV Gliosis	0	–	+	–	–
HCP3	M	17	Term	No	–	1	2	Right	CE	3	+	+	+	+
HCP4	M	10	Term	No	–	1	2	Right	PVIH	1	+	+	+	+
HCP5	F	14	28	No	–	1	2	Right	Parenchymal defect	2	–	+	–	–
HCP6	M	14	Term	No	–	1	2	Right	PVHI	3	–	+	+	–
HCP7	M	7	23	No	–	1	1	Left	No lesion	0	–	–	–	–
HCP8	F	10	Term	No	–	1	1	Left	Mild parenchymal atrophy	1	–	+	–	–
HCP9	M	17	Term	Yes[a]	Anticonvulsant	1	2	Left	CE	3	–	+	–	+
HCP10	F	13	Term	Yes	Anticonvulsant	1	1	Left	PV-WMI	1	–	+	–	–

Patient demographic includes gender; age in years; gestational age (GA) in weeks [term (> 37 weeks)]; presence of epilepsy; medications; Gross Motor Function Classification System (GMFCS) level; Manual Abilities Classification Scale (MACS) level; the MA hemisphere; the lesion type and location along with possible extension of the lesion. Lesion size 0: no lesion; lesion type 1: spot-type lesion; lesion size 2: noticeable abnormality; lesion size 3: major lesion. Symbol '+' indicates the lesion was located in the specific area, while '-' indicates the absence of a lesion. PV-WMI: Periventricular White Matter Injury; PV Gliosis: Periventricular Gliosis; CE: Cystic Encephalomalacia; PVIH: Periventricular Intraventricular Hemorrhage: PVHI, Periventricular Hemorrhagic Venous Infarction; Th: Thalamus; PW: Periventricular White Matter; IC: Internal Capsule; BS: Brainstem.

[a] Patient has been seizure free for 13 years.

(D3), and little (D5) finger of both hands using von Frey monofilaments (tactile™ sensory evaluator, Fabrication Enterprises, NY) (Keizer et al., 2008). We asked participants to place their hands on their lap, palmar surface up, and close their eyes. The three digits were stimulated in a pseudo-randomized order with a range of monofilaments (4, 6, and 8 g). Each of the testing digits was touched seven times for each monofilament. Testing started with monofilaments of 4 g and was increased until successful tests were achieved. Normal touch (score: 1) was achieved when the responses were accurate at least 5 times for the specific digit for monofilaments of 4 g; fair (score: 2) when the responses were accurate for at least 3 times for monofilaments of 4 g or at least 5 times for monofilaments of 6 g; and poor (score: 3) for all remaining scores. Detailed description of the procedure can be found elsewhere (Riquelme and Montoya, 2010).

Static and moving two-point discrimination was assessed using the Touch Test® Two-Point Discriminator (Exacta™ Evaluation Kit; North Coast Medical Inc., CA). Either a two-point or one-point stimulus was applied randomly to the tip of D1, D3, and D5. The participant was asked to state whether he/she perceived a one- or two-points stimulus. A range of two-point stimuli was used having a distance of 5, 8, and 11 mm respectively between the stimulation points. Testing started with the 5 mm two-point stimulus. Each testing digit was touched seven times. If responses were inaccurate, the distance between the points was increased until successful tests were achieved. The test for the specific finger was regarded as successful if four out of seven responses were accurate. The score interpretation was based on guidelines of the American Society for Surgery of the Hand (Hunter et al., 1995; Lee Dellon, 1997): normal discrimination (score: 1) was achieved when the responses were accurate for 5 mm, fair (score: 2) for 8 mm, and poor (score: 3) for 11 mm. For the moving two-point discrimination test, we applied the point(s) to the distal interphalangeal joint on the palmar surface of the hand and slowly moved them distally to the fingertip. Participants were asked to identify whether one or two points were perceived. The same scoring was followed as in the static two-point discrimination test.

2.3. MEG acquisition and experimental paradigm

Somatosensory Evoked Fields (SEF) were collected with a partial coverage (76-axial gradiometers) pediatric MEG system (BabySQUID Tristan Technologies, Inc., CA) (Okada et al., 2006) that is located inside a magnetically shielded room (MSR) (Imedco, Hägendorf, Switzerland). We used the BabySQUID system because it has specific technical characteristics, which are appealing for our study's focus: (i) the gap between the detection coils and the headrest is approximately half the gap of conventional adult MEG systems, making signal strengths at the sensors stronger by a factor of about four; and (ii) the sensor array has higher density compared to the conventional MEG systems (12–14 mm sensor spacing instead of 30–40 mm) offering a spatial resolution of 3–4 times higher than the conventional adult MEG systems (Okada et al., 2006). High spatial resolution is crucial for mapping accurately the functional representation of S1. The SEF were recorded from the contralateral hemisphere to tactile stimulation of D1, D3, and D5 at a sampling rate of 1024 Hz. Both hands were stimulated in consequent recording sessions. The tactile stimuli were delivered through thin elastic membranes attached to the distal, volar parts of the three digits. The membranes were inflated with compressed air pulses through rigid plastic tubes using the Somatosensory Stimulus Generator (4D NeuroImaging Inc., CA). The skin at the tip of D1, D3, and D5, was gently tapped. The compressed air pulses were released with an interstimulus interval of 1.5 ± 0.5 s following a pseudorandom order. The pressure of the tactile stimulator rose to 0.10 bar overpressure in 10 ms.

Each finger received at least 180 stimuli in total. The actual MEG recordings lasted ~12 min per hand; total duration of actual MEG recording was ~24 min. Stimulations were delivered in consecutive short-duration (6 min) runs with 60 stimuli per finger (180 stimuli in total). Before the recordings, the children spent time in the facility to become accustomed to the environment. Children were awake during the recordings and able to stay still during each session staring into the face of a cartoon placed on the walls of the MSR. The child could terminate the study at any time. One researcher (C.P.) was always present in the MSR. If necessary, the child's parent was also inside the MSR to make the child feel more at ease with the procedure. If excessive movements were observed, the session was repeated.

2.4. MRI/DTI acquisition

We performed the MRI examinations with a 3 T Magnetom Tim Trio (Siemens Healthcare, Germany). The imaging protocol consisted of structural and diffusion-weighted sequences. The structural sequence was a T1-weighted high-resolution magnetization-prepared rapid-acquisition gradient-echo acquisition, which used volumetric echo-planar (EP) imaging navigators for real time motion correction [voxel size (mm) = 1.0 × 1.0 × 1.0; field of view (FOV) = 19.2–22.0 cm; echo time (TE) = 1.74 ms; repetition time (TR) = 2520 ms; flip angle = 7°]. Volumetric T2-SPACE acquisition was prescribed sagittally with isotropic voxel size of 1 mm^3. The FOV was set to 256 mm and matrix size was 256. TR = 3200 ms, TE = 363 ms, GRAPPA acceleration R = 2, echo-spacing of 3.63 ms for a total imaging time of 3:23 min. The diffusion sequence (prescribed axially) used EP readouts [voxel size (mm) = 2.0 × 2.0 × 2.0; FOV = 11–12.8 cm; TE = 88 ms; TR = 8320–10,934 ms; flip angle = 90°; 30 gradient diffusion directions at b = 1000 s/mm^2; 10 acquisitions with b = 0 s/mm^2].

2.5. Identification of less and more affected hemispheres

A pediatric radiologist (P.E.G.) reviewed the MRI scans. For each child, a MA and a less affected (LA) hemisphere were defined. The MA hemisphere referred to the hemisphere where structural abnormalities were detected, which was always contralateral to the motor impairment in the children with HCP. In the one case where no structural abnormalities were observed in the MRIs (HCP7), the MA hemisphere was defined as the hemisphere contralateral to the hand with the lower degree of residual motor function. To balance out possible inherent differences in the functioning of the left and right hemispheres (Pihko et al., 2014), each child in the TD group was assigned a randomly selected hemisphere (1 or 2). Each hemisphere was assigned a random value between 0 and 1 using a random number generator function. These values were then sorted from 0 to 1 and divided into two separate hemisphere groups designated as randomly selected TD hemispheres 1 and 2. This classification was applied to all MEG and DTI measures.

2.6. MEG data analysis at sensor level

We analyzed the MEG data with Brainstorm (Tadel et al., 2011). Raw data were inspected for bad sensor recordings. Then, the data were segmented into trials from − 100 to 400 ms relative to the stimulus onset. For each trial, the direct current offset was removed and the data were filtered between 1 and 100 Hz. A notch filter was also applied at 60 Hz. Trials contaminated with artifacts were rejected. The remaining trials were kept for further analysis. These trials were then averaged (∼60 trials for each stimulation site) for each separate run. Grand averages across all runs were estimated per stimulation site for each participant. There was no significant difference in the number of useful trials between stimulation sites or groups ($p > 0.05$). The peak latency of the first cortical response was determined visually from the grand average plot for each stimulation site and each participant.

2.7. MEG co-registration

Co-registration was performed using an in-house procedure that is described in details in Papadelis et al. (2011). The procedure combines information from the FASTRACK (Polhemus, VT, USA) and the Polaris (Polaris, Northern Digital Inc., Canada) tracking systems. Prior to the experiment, the child was asked to sit on a special chair where the FASTRAK transmitter was attached. The FASTRAK receiver was then placed securely on the child's head with a headband. With a non-toxic washable marker, fifteen anatomical landmarks were marked on the child's face, such as the nasion, left and right pre-auricular points, points on the forehead, and the tip of the nose. These anatomical landmarks were digitally marked by the experimenter using the stylus of the FASTRAK system. Beyond these landmarks, additional points (∼300) were recorded from the child's scalp. The child was then transferred to the MSR and instructed to lie on the bed of the BabySQUID cart (Okada et al., 2006; Papadelis et al., 2011). The experimenter placed the child's head on the BabySQUID headrest and digitized the previously marked anatomical landmarks using the Polaris system that is located inside the MSR. The experimenter was always in the MSR and monitored the child during the recording. If the experimenter noticed that the child moved his/her head during the run, the recording was repeated. Co-registration between the MEG and MRI data was achieved by aligning the two sets of points derived from the two tracking systems (FASTRACK and Polaris) and fitting them to the child's scalp surface by a surface-matching technique. High quality SEF with a coregistration error of < 0.5 mm were obtained for both hemispheres in all children with HCP and eleven TD children; for two TD children, MEG data were recorded from one hemisphere (one for the left and one for the right hemisphere). The MEG data from these two children were excluded from further analysis.

2.8. MEG data analysis at source space

For source localization, we estimated the current density maps using the depth-weighted minimum norm estimation (wMNE) (Baillet et al., 2001) at the peak of the first cortical response after the stimulus onset obtained for each run, stimulus site, and participant. MNE has been previously used by our group and other researchers in single sensor or partial-coverage MEG systems for the localization of brain activity in healthy and sick children and adults (Hämäläinen and Ilmoniemi, 1984; Ahlfors et al., 1992; Papadelis et al., 2013, 2014; Khan et al., 2014; Hunold et al., 2014). For the wMNE estimation, the default parameters were used. The current density maps were averaged across runs for each stimulus site and participant.

For the forward model, we computed realistic head models as boundary element models (BEM) consisting of four surface layers (brain, inner skull, outer skull, and head surface) that were reconstructed from individual structural T1 MRI scans. The models were generated with the OpenMEEG software (Gramfort et al., 2010) using the adaptive integration method. The wMNE were estimated both at the cortex surface (∼15,000 sources) as well as the brain volume (∼20,600 sources). Cortical reconstruction and volumetric segmentation was performed using Freesurfer (Dale et al., 1999; Fischl, 2012). The noise covariance matrix was computed from − 100 to 0 ms. In order to assess the confidence interval of our localization findings, we also calculated the current density maps for each run separately, and defined the location of the maximum activity at the peak of the first response after tactile stimulation. For each run (containing ≤ 50% of all trials), we then estimated the distance of this location from the location of maximum activity when all runs were combined together. This distance was estimated for each digit, hemisphere, and participant. Outliers were removed from further analysis. The mean distance (± S.D.) was defined as the confidence interval of our localization findings (in mm). In all recordings, the maximum activity at the peak of the first cortical response was localized in brain areas, which were well-covered by our system's sensory array.

2.9. MEG-defined regions of interest

For every child and every stimulation site, we defined a region of interest (ROI) at the maxima of the current density maps during the peak of the first cortical response after the stimulus onset. The ROIs were defined both at the cortex as well as at the volume space; henceforth, they will be referred to as cortical and volumetric MEG-defined ROIs, respectively. Each volumetric MEG-defined ROI consisted of 27 voxels (forming a 3 × 3 × 3 voxel cube) surrounding the voxel with the global maxima. Each cortical MEG-defined ROI consisted of ten neighboring vertices surrounding the vertex with the maximum activation. The coordinates of the cortical and volumetric MEG-defined ROIs were transformed into the MNI space. The Euclidean distances between the MNI coordinates of the volumetric MEG-defined ROIs for the three stimulated fingers were estimated for each hemisphere and each individual. A virtual sensor was defined at the location of each cortical MEG-defined ROI. The latency and amplitude at the peak of the first cortical response after stimulus onset were calculated for each virtual sensor.

2.10. MEG time frequency analysis (TFA)

TFA of MEG activity at the virtual sensors was quantified by complex Morlet wavelet analysis, which demonstrates both phase-locked and non-phased locked changes in power at different frequencies over time. The analysis was performed with Brainstorm (Tadel et al., 2011). The Morlet wavelets with a width of five circles per wavelet at center frequencies between 1 and 100 Hz, in 1 Hz steps, were applied to the averaged source waveforms of each run of each finger, for each child. The resulting time-frequency representations were corrected with respect to the baseline activity from − 50 to 0 ms to calculate the relative power changes. Power changes in the TFA will be described as event-related synchronization (ERS) or event-related desynchronization (ERD) depending on whether oscillatory power was increased or decreased after the stimulus onset compared to baseline (Aranibar and Pfurtscheller, 1978).

2.11. Probabilistic tractography analysis

The PDT algorithm we used is described elsewhere (Behrens et al., 2007). First, we reconstructed the AST of the three digits per hemisphere in each participant. Then, we estimated the mean diffusion parameters of fractional anisotropy (FA), axial diffusivity (AD), mean diffusivity or apparent diffusion coefficient (ADC), and radial diffusivity (RD) (Soares et al., 2013) within the reconstructed AST in each participant. For the AST reconstruction, we used the Functional MRI of the Brain toolbox (FMRIB) (http://www.fmrib.ox.ac.uk.fsl). For each child, we extracted the diffusion gradients and the corresponding b-values from the DICOM files. Eddy current, motion and distortion correction, as well as brain extraction of the diffusion data were performed using FSL (Woolrich et al., 2009). The diffusion data from one child with HCP (HCP7) and one TD child were excluded from further analysis due to motion artifacts. Nine children with HCP and ten TD children were included in the DTI analysis. For each child, the T1-image was transformed to the diffusion space. The volumetric MEG-defined ROIs were transformed from the MNI space to the diffusion space. Within FSL, we ran BEDPOSTX (Bayesian Estimation of Diffusion Parameters Obtained using Sampling Techniques for Crossing Fibers) on each child's diffusion weighted volumes to model crossing fibers within each voxel. For the PDT, we used the volumetric MEG-defined ROIs as seed regions and the thalamus and brainstem as target regions within the same hemisphere. The thalamus and brainstem were automatically segmented using Freesurfer, and manually modified using an MRI-atlas as reference (Oishi et al., 2011). We then used the PDT algorithm to trace the AST from the MEG-defined ROI to the thalamus and brainstem. The tractography algorithm drew 5000 samples going from each voxel in the seed region to the target regions. The output was a probabilistic map that provided, at each voxel, a connectivity value, corresponding to the total number of samples that passed from the seed region through that voxel to the target regions. Each probabilistic map was then thresholded to include voxels with values 10% or more of the maximum connectivity value (Guye et al., 2003; Ciccarelli et al., 2006). The thresholded probabilistic maps were then transformed into binary images. For each child, three binary images corresponding to the stimulated digits (D1, D3, and D5) were generated to reconstruct the AST for each hemisphere. To assess the AST diffusion parameters, we masked the diffusion parameter maps (FA, AD, ADC, and RD) using the corresponding binary images. The masked maps were then used to estimate the mean diffusion parameters for each child and each hemisphere.

2.12. Statistical analysis

Statistical analysis was performed using SPSS 23.0 (SPSS Inc., IL, USA). We compared the latency and amplitude of the M50, as extracted from the virtual sensors, with a mixed 2 (group: HCP, TD) × 2 (hemisphere: MA, LA) analysis of variance (ANOVA), with group being a between-subject factor and hemisphere a within-subjects factor. The digit (D1, D3, and D5) was added as another within-subjects factor (mixed 2 × 2 × 3 ANOVA). We also compared the Euclidean distances between the different digits with a mixed 2 (group: HCP, TD) × 2 (hemisphere: MA, LA) ANOVA with group being a between-groups factor and hemisphere a within-subjects factor. The pair of digits was added as another within-subjects factor (mixed 2 × 2 × 2 ANOVA). For the TFA, we performed a statistical analysis of the time-frequency representations of the event-related power changes both within-subjects (LA vs. MA for the children with HCP) as well as between-subjects (HCP vs. TD). All statistical tests were employed using Monte Carlo permutation tests (here: 5000 permutations). The arising multiple-comparison problem was corrected with cluster-based statistical analysis (Maris and Oostenveld, 2007). Statistical analysis for the TFA was performed separately for each digit. For the diffusion parameters, we compared the mean FA, AD, ADC, and RD of the AST across each hand's digits with a mixed 2 (group: HCP, TD) × 2 (hemisphere: MA, LA) ANOVA, with group being a between-subject factor and hemisphere a within-subjects factor. For all aforementioned ANOVA tests, normality assumption was tested with the Shapiro-Wilk test, sphericity assumption with the Mauchly test, and equality of variances with the Levene test. The level of significance was set at $p < 0.05$ unless otherwise stated. We also correlated the features of MEG data (i.e. latency and amplitude of M50, Euclidean distances between cortical responses of different digits, and the relative power changes in TFA) with the diffusion parameters of the contralateral AST (mean values of FA, AD, ADC, and RD) using Pearson's correlation. Finally, we correlated the behavioral measures (mean scores of somatosensory tests for the MA and LA hand of each child with HCP) with the features of the MEG data and the AST diffusion parameters of their MA and LA hemisphere using Pearson's correlation. Statistical significance was set at $p < 0.05$.

3. Results

3.1. MRIs

Table 1 presents the type, size, location, and extent of the brain lesion for the children with HCP, based on structural MRI. Three children with HCP had large unilateral lesions involving the frontal and temporal lobes, as well as a portion of the basal ganglia and thalamus, six children had periventricular white matter injury, and one child had no lesion or gross structural abnormality observed on the MRI. No structural abnormalities were observed in the MRIs of the TD children.

3.2. Behavioral measures

Fig. 1 presents the scores of the static and moving two-point discrimination tests for each digit for the MA and LA hemispheres. Six children with HCP had mildly abnormal findings (i.e., score: 2) in the MA hand for either the static (5 children for D1; 4 children for D3; 4 children for D5) or the moving (2 children for D1; 6 children with D3; 4 children with D5) two-point discrimination tests for at least one digit. Out of these six children, one child also had mildly abnormal findings (score: 2) in the LA hand for both tests. Four children with HCP had normal findings (score: 1) in both hands for both tests. All children with HCP presented normal findings for the monofilament tests (score: 1). All TD children had normal findings for both discrimination tests and the monofilament tests for both hands.

3.3. Latency and amplitude of the earliest cortical response

Tactile stimulation of all digits for both hands evoked the earliest cortical response for all TD children at ~40–50 ms (M50 component). The mean latency and amplitude of M50 for the children with HCP and the TD children are presented in Table 2. We did not observe significant differences in the latency or the amplitude of M50 between the MA and the LA hemispheres of children with HCP. We also did not observe differences in the latency nor the amplitude between the children with HCP and the TD children. However, in the three children with HCP who

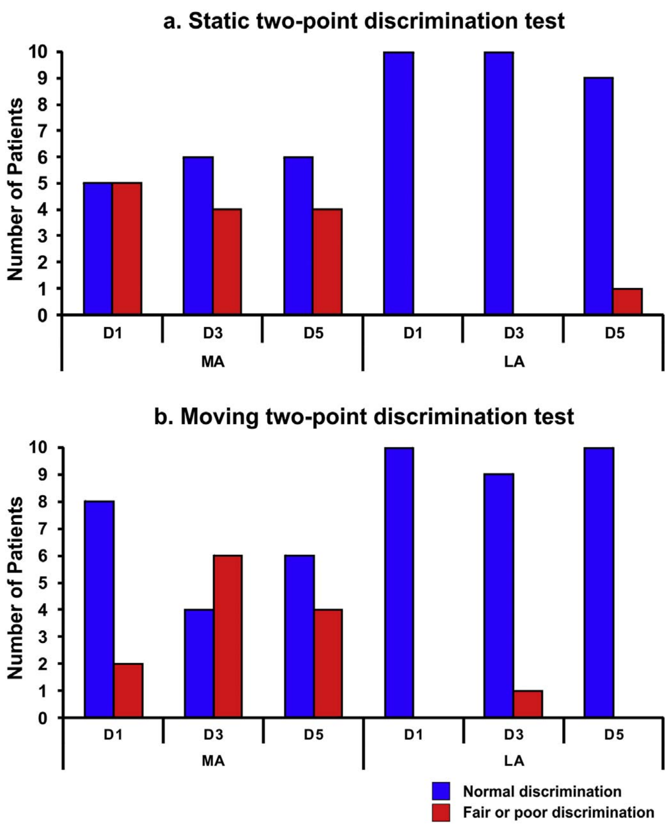

Fig. 1. Static and moving two-point discrimination tests. (a) Number of patients with normal (score 1) (blue bars) and fair or poor (scores 2 or 3) (red bars) static two-point discrimination for each digit (D1, D3, and D5) for the MA and LA hemispheres of children with HCP. (b) Number of patients with normal (score 1) (blue bars) and fair or poor (scores 2 or 3) (red bars) moving two-point discrimination for each digit for the MA and LA hemispheres of children with HCP. (For interpretation of the references to color in this figure legend, the reader is referred to the web version of this article.)

have large lesions (lesion size = 3) in their MRIs we observed a remarkable M50 latency delay for the MA compared to the LA hemisphere (mean delay for all digits: 23.1 ± 18.6 ms) (see Fig. 2 for the SEFs of one of these participants). For the three children with large lesions, the mean latency for the MA hemisphere was: 63.16 ± 16.85 ms for D1, 65.43 ± 16.68 ms for D3, and 60.23 ± 14.2 ms for D5. For the LA hemisphere it was: 38.13 ± 3.49 ms for D1, 42.0 ± 10.17 ms for D3, and 39.4 ± 9.81 ms for D5.

3.4. Source localization of M50

In five children with HCP, the maximum activity of wMNE at the peak of M50 was localized in the precentral gyrus of the MA hemisphere for either all digits or at least one digit. Fig. 2 presents the localization findings for one representative participant. All other maximum wMNE activities were localized in the postcentral gyrus. All children with HCP showed an abnormal topography in either one or both hemispheres (see Fig. 3b). For the TD children, the M50 current sources in the contralateral S1 agreed with the known somatotopy of the sensory homunculus: D1 medial and superior to D3 and D5. The confidence interval of our localization findings was 15.36 ± 7.89 mm. No significant difference was observed between the confidence intervals of localization for the children with HCP and the TD children.

3.5. Euclidean distances

Fig. 3 presents the mean Euclidean distances for the two hemispheres of the TD group and the group with HCP children for all pairs of digits. Table 3 presents the Euclidean distances for all participants. Euclidean distances between the first cortical responses to tactile stimulation of D1, D3, and D5 were longer in the HCP (for the MA hemisphere: 11.18 ± 8.83 mm; for the LA hemisphere: 11.99 ± 8.61 mm) compared to the TD group (randomly selected hemisphere 1: 7.15 ± 4.66 mm; randomly selected hemisphere 2: 7.94 ± 4.79 mm) for both hemispheres [$F_{1,19} = 4.945$; $p = 0.038$]. The main effect of hemisphere [$F_{1,19} = 0.392$; $p = 0.539$] and the interaction effect (hemisphere x group) [$F_{1,19} = 0.00$; $p = 0.985$] were not significant, indicating that the group difference was of similar magnitude for the MA and LA hemispheres.

3.6. Time frequency analysis results

We observed an ERS at the virtual sensor in the S1 for both hemispheres of TD children and children with HCP in beta (from ~15 to 30 Hz) and gamma (from 30 to ~65 Hz) frequency bands from ~10 to ~120 ms after the stimulus onset. Fig. 4 presents the relative power changes (for digit D1) for a randomly selected hemisphere of TD children (a), and the LA (HCP-LA) (b), and MA hemispheres (HCP-MA) (c) of children with HCP. No differences were observed ($p > 0.05$) between the LA and MA hemispheres of children with HCP (Fig. 4d). For early latencies up to ~100 ms, we observed a significant suppression ($p < 0.05$) in the gamma frequency band ranging from ~45 to ~60 Hz for the LA hemisphere of children with HCP (HCP-LA) compared to a randomly selected hemisphere of TD children. Gamma-band suppression ($p < 0.02$) ranging from ~45 to ~75 Hz was also seen between the MA hemisphere of children with HCP compared to the TD children

Table 2
Latency and amplitude at the peak of M50.

	D1		D3		D5	
	MA	LA	MA	LA	MA	LA
Latency (ms)						
HCP	46	44.1	46.1	45	44.6	43.4
(n = 10)	(± 14.8)	(± 7.7)	(± 16.1)	(± 9.5)	(± 14.3)	(± 7.7)
TD	45.6	44.7	46	45.6	45	43.8
(n = 11)	(± 4.4)	(± 5.1)	(± 6.8)	(± 5.3)	(± 5.3)	(± 6.2)
Amplitude (nA-m)						
HCP	122.6	99.2	105	92	118.1	117.6
(n = 10)	(± 126.1)	(± 64.1)	(± 115.4)	(± 97.4)	(± 132.4)	(± 139.7)
TD	96.0	126.0	110.5	159.8	145.3	169.2
(n = 11)	(± 64.3)	(± 76.1)	(± 67.5)	(± 88.2)	(± 92.1)	(± 136.4)

Mean (± S.D.) latency (in ms) and amplitude (in nA-m) at the peak of M50 for the SEFs of the three digits (D1, D3, and D5) for the MA and LA hemispheres of HCP and randomly assigned hemispheres of TD children.

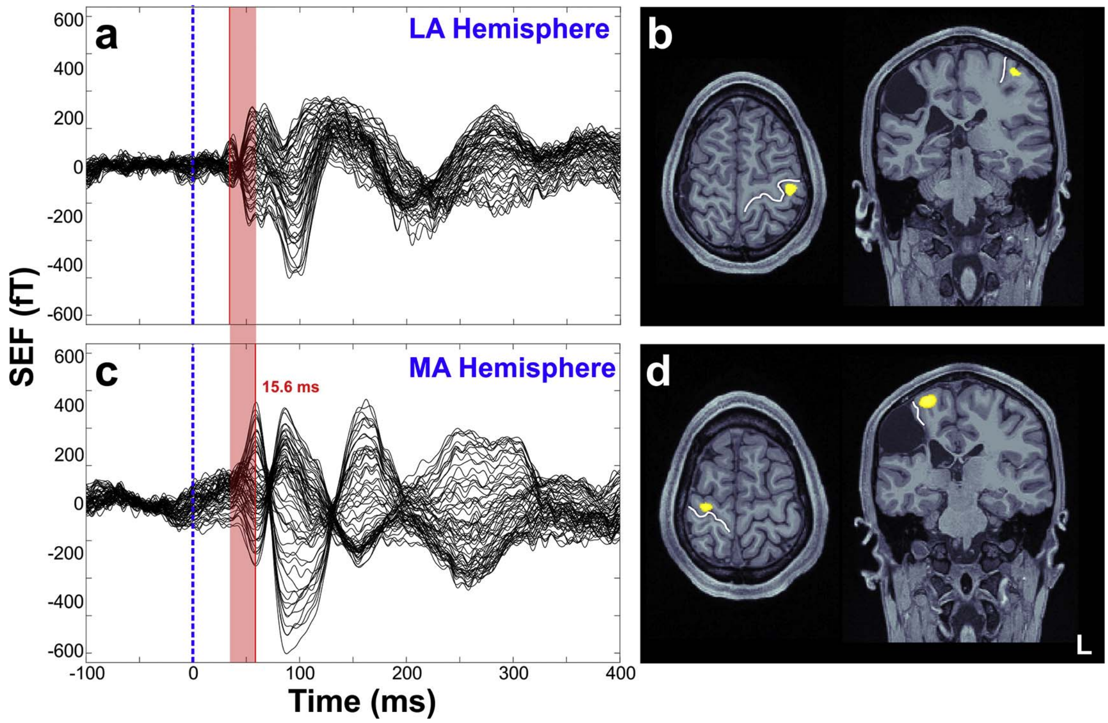

Fig. 2. SEFs and localization at the M50 peak for a child with HCP. (a & c) SEFs elicited by tactile stimulation of the child's right (a) and left (c) little fingers corresponding to the LA and the MA hemispheres respectively. Data from CP3 having a large unilateral lesion in the right hemisphere. Red line indicates the delay (15.6 ms) of the M50 peak for the MA (compared to the LA) hemisphere. (b & d) Source localization (wMNE thresholded at 90%) at the peak of the first cortical response for the LA (b) and MA (d) hemispheres for D5. The white line indicates the central sulcus. (For interpretation of the references to color in this figure legend, the reader is referred to the web version of this article.)

for latencies up to 100 ms after the stimulus onset.

3.7. AST diffusion parameters

Fig. 5(a & c) presents the MEG-defined (for digits D1, D3, and D5) and anatomically-defined ROIs overlaid on a 3D representation of T1 (a) and on a representation of the FA maps (c) for a child with HCP (HCP3). Fig. 5(b & d) also shows the binary images of the thresholded probabilistic maps of AST for a TD child (b) and a child with HCP (d) for D1, D3, and D5. The mean FA, AD, ADC, and RD values for the AST in the TD children and the children with HCP are shown in Fig. 6. We observed a significant increase of mean ADC in the HCP compared to the TD group [$F_{1,17} = 8.123$; $p = 0.011$] for both hemispheres. The main effect of hemisphere [$F_{1,17} = 7.353$; $p = 0.015$] and the interaction effect (hemisphere x group) [$F_{1,17} = 4.704$; $p = 0.045$] were also significant for the mean ADC. Significant differences were also observed for the mean ADC between the MA and LA hemispheres ($p = 0.014$) of children with HCP (Fig. 6). The mean RD was also significantly higher for the HCP compared to the TD group [$F_{1,17} = 14.848$; $p = 0.001$] for both hemispheres. We also observed a main effect of hemisphere [$F_{1,17} = 5.09$; p = 0.038] for the mean RD but not the interaction effect (hemisphere x group) [$F_{1,17} = 1.241$; $p = 0.281$].

3.8. Correlation of MEG features with diffusion parameters of AST

Pearson test showed a positive correlation between the latency of M50 component and the mean AD of the AST in the MA hemisphere for all three digits: D1 [R = 0.673; $p = 0.002$; D3 [R = 0.710; p = 0.001]; and D5 [R = 0.644; $p = 0.004$]. We also observed a positive correlation between the amplitude of M50 and the mean ADC [for D1: R = 0.465; p = 0.045] as well as the mean RD [for D1: R = 0.601; $p = 0.006$; for D3: R = 0.546; $p = 0.016$; for D5: R = 0.540; $p = 0.017$] of the AST in the MA hemisphere. Pearson test also showed a negative correlation between the relative power change in the gamma band and the mean AD [R = − 0.615; $p = 0.005$] of the AST for the MA hemisphere. No significant correlations were observed between the mean FA, ADC, RD, and the Euclidean distances.

3.9. Correlation of MEG features with sensory tests

We observed a positive correlation between the Euclidian distances and the static [D1–D3 with sensory tests in D3: R = 0.884; $p = 0.001$; D1–D5 with sensory tests in D5: R = 0.775; $p = 0.008$] as well as moving [D1–D5 with sensory tests in D1: R = 0.703; $p = 0.023$; D1–D5 with sensory tests in D5: R = 0.778; $p = 0.008$] two-point discrimination tests for the MA hemisphere of children with HCP. No significant correlations were observed between the rest of the MEG features (i.e. latency and amplitude of M50, and relative power changes) and the sensory tests.

3.10. Correlation of diffusion parameters of AST with sensory tests

Pearson test showed a positive correlation between the mean AD and the static [R = 0.786; $p = 0.012$] as well as moving two-point discrimination test [R = 0.667; $p = 0.05$] for the MA hemisphere. No significant correlations were observed between the mean FA, ADC, RD, and the sensory tests.

4. Discussion

For the first time we associate bilateral functional reorganization in the S1 with abnormalities in the structural integrity of the AST in the same cohort of children with HCP. In addition, we correlate these abnormalities with behaviorally-assessed sensory deficits. Our MEG data showed: (i) a shift of the S1 anteriorly into the precentral gyrus for the MA hemisphere of five out of ten children with HCP for at least one digit; (ii) an abnormal somatotopic organization in all children with HCP in either one or both of their hemispheres; (iii) longer Euclidean distances between the cortical responses to tactile stimulation of the first, third, and fifth digits in the children with HCP compared to the TD

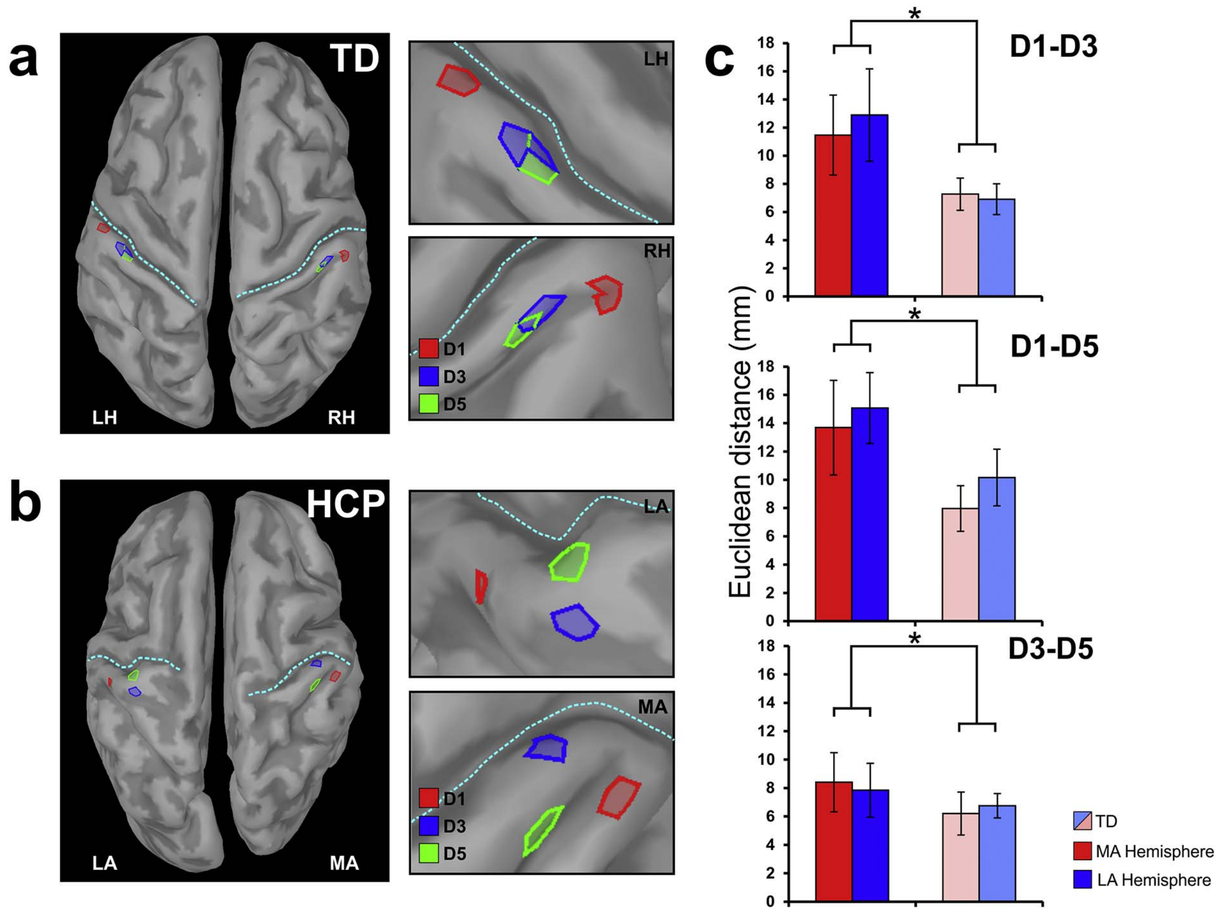

Fig. 3. Cortical mapping of S1 and Euclidean distances for children with HCP and TD children. (a & b) Cortical mapping at the peak of M50 for tactile stimulation of D1 (red), D3 (blue), and D5 (green) for a TD child (a) and a child with HCP (b) (HCP1). Brain activity is displayed at the extracted cortical surface for clarity. LH: left hemisphere; RH: right hemisphere. (c) Average Euclidean distances (in mm) for all pairs of digits (D1–D3; D1–D5; D3–D5) for children with HCP (red and blue indicate MA and LA hemispheres respectively) and TD children (light red/blue indicate randomly selected hemispheres). Statistical significant differences between groups are indicated with asterisks (*) [$p < 0.05$; main effect of ANOVA]. (For interpretation of the references to color in this figure legend, the reader is referred to the web version of this article.)

children; (iv) suppressed gamma responses in the SEFs at early latencies for both hemispheres of children with HCP compared to TD children; and (v) a positive correlation between the Euclidian distances and the behaviorally-assessed sensory tests for the MA hemisphere of children with HCP. Our MEG-guided PDT data showed: (i) higher ADC (or mean diffusivity) and RD values of the AST in children with HCP compared to TD children; and (ii) a positive correlation between the AD of the AST with the static and moving two-point discrimination tests in children with HCP. Correlation analysis between the MEG and MEG-guided PDT data showed: (i) a positive correlation between the M50 latency and the AD; (ii) a positive correlation between the M50 amplitude and the ADC and RD; and (iii) a negative correlation between the relative power change in the gamma frequency band and the AD of the AST for the MA hemisphere.

4.1. Abnormal somatotopy and longer distances between digit representations

Our MEG findings suggest bilateral reorganization of the finger representation at the cortical level in the brains of children with HCP. For TD children, S1 somatotopy was similar to that previously shown with MEG (Hari et al., 1993; Nakamura et al., 1998) and fMRI (Maldjian et al., 1999). An abnormal somatotopic organization was observed in all children with HCP in either one (ipsilesional in two children) or both of their hemispheres. Moreover, Euclidean distances between the first cortical responses were significantly longer in the HCP group compared to the TD group. The distances for the TD were within the range of previously reported values. For instance, the D1–D5 distance was 9.06 ± 5.98 mm compared to 3.2 mm in Hlustík et al. (2001) and 18 mm in Maldjian et al. (1999). The Euclidean distance of the somatotopic finger representation in S1 represents an important metric for neuroplastic reorganization (Sterr et al., 1998; Candia et al., 2003). We regarded the Euclidean distance arrangement D1–D3 < D1–D5 and D3–D5 < D1–D5 as representing normal somatotopic representation because it is congruent with the peripheral finger distance profile and, consequently, with the well-accepted concept of homuncular cortical representations for the sensory cortex (Candia et al., 2003). Previous studies have reported significant differences in the distance of digit representations in S1 between children with CP and TD children (Nevalainen et al., 2012; Papadelis et al., 2014) but with contradictory findings. More specifically, in our previous study in a small cohort of children with CP (Papadelis et al., 2014), we observed longer distances of digit representations in S1 but only for the MA hemisphere. In contrast, Nevalainen et al. (2012) found that the representation areas of D2 and D5 were closer to each other in both hemispheres in participants with spastic HCP than in healthy controls. Here, we observed significantly longer distances between the representation areas of D1, D3, and D5 for the children with HCP compared to the TD children, independent of the hemisphere. Moreover, Euclidian distances were positively correlated with both the static as well as the moving, behaviorally-assessed sensory tests for the MA hemisphere of children with HCP. Thus, longer distances between the cortical representations of different fingers were indicating more severe sensory deficits in the paretic hand of children with HCP. Our findings suggest a maladaptive

Table 3
Euclidian distances.

	D1–D3		D1–D5		D3–D5	
	MA	LA	MA	LA	MA	LA
HCP1	14.15	12.02	22.80	13.57	14.97	2.24
HCP2	11.8	11.76	12.45	11.72	2.2	19.99
HCP3	4.06	11.28	1.64	12.66	3.66	8.45
HCP4	3.84	3.46	4.78	7.65	8.0	4.65
HCP5	12.15	28.50	18.68	21.87	6.55	16.38
HCP6	14.7	1.22	4.30	7.81	13.93	6.71
HCP7	2.39	9.14	22.89	13.14	22.2	4.97
HCP8	33.23	33.00	32.66	32.00	2.15	1.22
HCP9	12.96	4.21	14.71	7.99	4.02	5.36
HCP10	5.36	14.29	1.97	22.32	6.42	8.51
	D1–D3		D1–D5		D3–D5	
	TD1	TD2	TD1	TD2	TD1	TD2
TD1	5.33	2.63	2.39	7.95	2.48	7.28
TD2	5.59	8.08	8.95	4.61	8.95	6.77
TD3	3.98	6.55	9.29	7.51	5.74	1.52
TD4	5.08	7.49	3.79	10.58	3.12	3.48
TD5	10.39	14.62	4.99	9.66	5.04	3.4
TD6	13.66	7.77	12.71	7.96	4.83	9.31
TD7	8.65	8.65	19.26	27.08	5.61	8.71
TD8	1.2	4.68	1.20	9.65	0.0	7.98
TD9	9.67	9.88	10.16	15.89	5.04	11.08
TD10	11.73	3.48	10.88	9.34	19.28	8.0
TD11	4.66	2.11	3.98	1.57	8.17	6.77

Euclidean distances (in mm) for all pairs of digits (D1–D3; D1–D5; D3–D5) for children with HCP and TD children.

change of body representation in the S1 of the MA hemisphere for children with HCP. Such a change has been previously reported in the brain of both animals and humans as a result of a change in limb usage caused by central nervous damage (for a review see Oouchida et al., 2016). The notion that longer distances between the cortical representations of different digits indicate a maladaptive change is in line with previous findings in musicians with focal hand dystonia (Candia et al., 2003). These previous findings showed a decrease of the Euclidean distances between the cortical representations of all the MA hand's fingers after therapy, which also resulted in a more orderly representation of the arrangement of those distances.

4.2. Shift of functional S1 to the precentral sulcus

In five children with HCP, the M50 was localized in the precentral gyrus of the MA hemisphere for at least one digit. To our best knowledge, it is the first time that displacement of sensory function to what is typically the motor cortex has been reported in a cohort of patients with CP. An exception is a single case of a 5-year-old boy with CP and epilepsy due to focal cortical dysplasia in whom a shift of the primary sensory region from the parietal to the anterior frontal lobe was observed for the MA hemisphere (Gondo et al., 2000). Somatosensory evoked magnetic responses up to 60 ms are well-known to be generated in S1 (Mauguière et al., 1997; Papadelis et al., 2011). In our participants, the distance between the precentral and the postcentral gyri was between 1 and 2 cm, well within the MEG localization abilities (Hari et al., 1988; Papadelis et al., 2009, 2011). However, the confidence interval of our localization findings was ~15 mm. Thus, it is plausible the shift of functional S1 to the precentral sulcus to actually reflect an expansion of MNE solutions from the actual primary generator located within the post-central gyrus to more anterior locations. MNE solutions of even focal sources can indeed extend across sulcal walls separated by only a few millimeters (Liu et al., 2002; Lin et al., 2006; Hauk et al., 2011). Moreover, errors in co-registration can affect the localization findings. Although these are plausible explanations, they are weakened by the fact that the shifts were observed only in children with HCP and for many children the shift was not observed for all digits. If the shift was due to an expansion of MNE or due to a co-registration error it will appear in all digits within the same run. Our data suggest a reorganization of S1, such that the sensory representation of some digits moved to the precentral gyrus, where the primary motor area is typically located. Such displacements of the sensory to the motor cortex, as demonstrated in the present study, are supported by the profound interconnectedness of the sensorimotor system, previously shown in both animal and humans (Rao et al., 1993; Porter, 1997; Pleger et al., 2003). Whether such a shift in the topological location of the somatosensory response to the precentral gyrus represents an adaptive or maladaptive process cannot be concluded by our findings. For example, previous EEG investigations in healthy adults have noted that Broadmann area 4 is involved in the processing of somatosensory information (Jung et al., 2008). Thus, instead of indicating a maladaptive change, the observed shift of cortical activity to the precentral gyrus may alternatively represent a compensatory change in the weighing of the neural networks

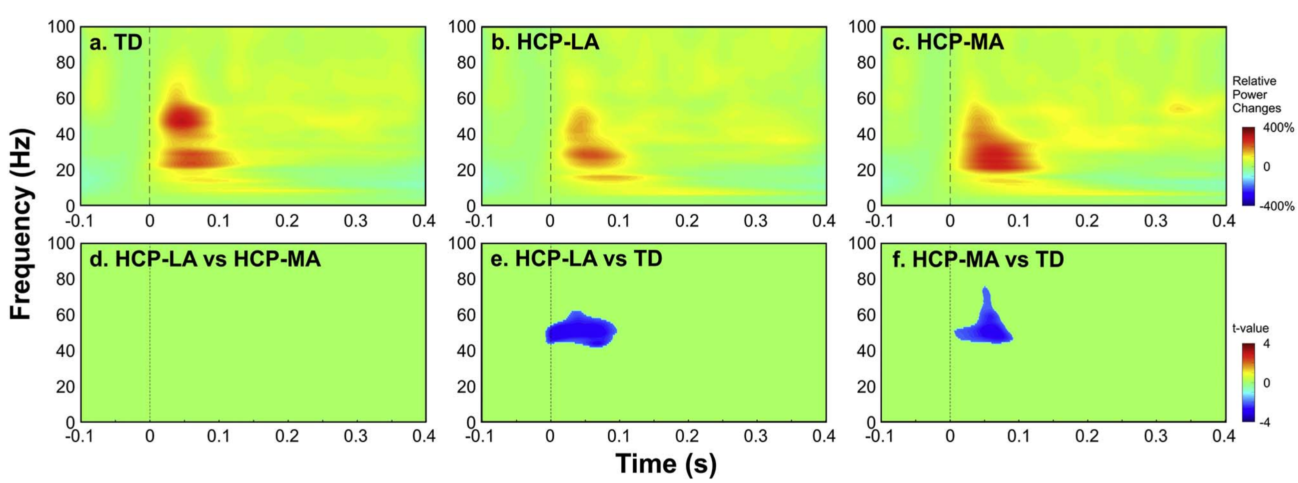

Fig. 4. Relative power changes in contralateral S1 for children with HCP and TD children. Time-frequency representations of relative power changes (baseline corrected from − 50 to 0 ms) estimated at a virtual channel located in contralateral S1. (a) Grand average of TFA for one randomly selected hemisphere of TD children; (b): grand average of TFA for the LA hemisphere of children with HCP; (c): grand average of TFA for the MA hemisphere of children with HCP. For the panels a, b, and c, warmer colors indicate stronger ERS, while colder colors indicate weaker ERD. (d) Statistical differences of the TFA between the LA (HCP-LA) and MA (HCP-MA) hemispheres of children with HCP; (e) between the LA hemisphere of children with HCP (HCP-LA) and a randomly selected hemisphere of TD children [$p < 0.05$; corrected for multiple comparisons]; and (f) between the MA hemisphere of children with HCP and a randomly selected hemisphere of TD children [$p < 0.02$; corrected for multiple comparisons]. The upper bar indicates the relative power change to the baseline power and the lower one indicates the t-value from statistical tests.

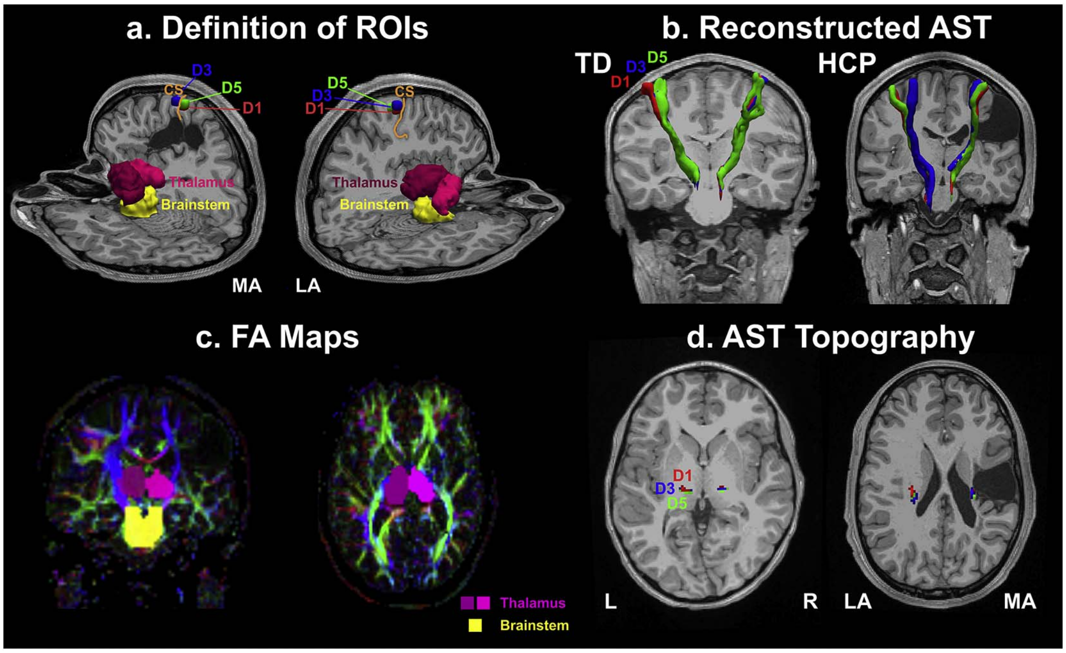

Fig. 5. ROIs and the corresponding AST. (a): MEG-defined ROIs (color-coded) for D1 (red), D3 (blue), and D5 (green), and anatomically-defined ROIs (right and left thalamus with lighter and darker purple, and brainstem with yellow) overlaid on a 3D representation of T1 for a child with HCP (HCP3). (b): The reconstructed AST [binary images of the thresholded (10%) probabilistic maps] for a TD child (9 years old girl) and a child with HCP (HCP3) for the three digits (D1: red; D3: blue; D5: green) overlaid on their MRIs (coronal and axial views). (c): Anatomically-defined ROIs (right and left thalamus with lighter and darker purple, and brainstem with yellow) overlaid on the FA maps for the same child as in (a). (d) Axial view of the AST (AST topography) at the level of thalamus for the three digits [D1 (red), D3 (blue), and D5 (green)] for the same child as in (a). (For interpretation of the references to color in this figure legend, the reader is referred to the web version of this article.)

that are involved in the processing of sensory information. Different weights in the neural network as a result of tactile feedback from mechanoreceptors in the skin and joints during development may explain why the shift was observed only in some and not all digits for a few patients with HCP.

4.3. Suppressed gamma responses in both hemispheres of children with HCP

Using time-frequency analysis, we tested whether the reactivity of the ongoing S1 activity in children with HCP differs between the LA and MA hemisphere or in comparison with TD children. Very few studies have examined the sensorimotor oscillatory responses to tactile or electrical stimuli of the upper limbs in children with CP (Guo et al., 2012; Pihko et al., 2014; Kurz et al., 2015a, 2015b). Except Guo et al.

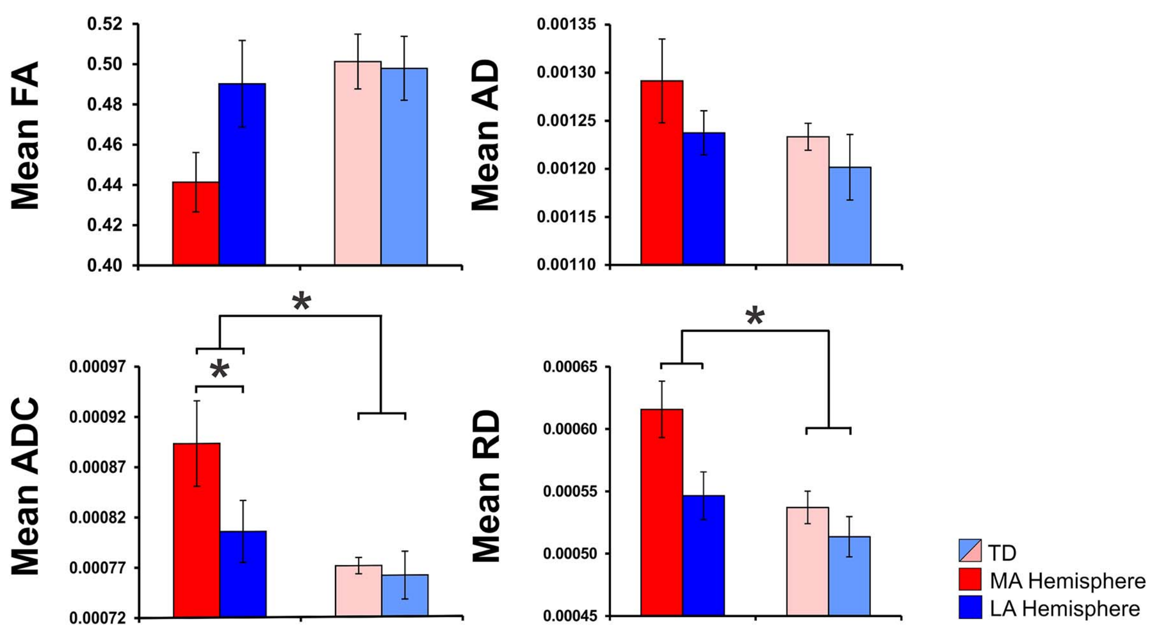

Fig. 6. Mean diffusion parameters for the AST in children with HCP and TD children. The graphs show the mean FA, AD, ADC, and RD values averaged for all digits (D1, D3, and D5) for the MA (red color) and LA (blue color) hemispheres of children with HCP and both hemispheres (light red and blue colors) of TD children. The error bars indicate the standard error of the mean. Statistical significant differences between groups are indicated with asterisks (*) ($p < 0.05$). (For interpretation of the references to color in this figure legend, the reader is referred to the web version of this article.)

(2012), prior studies have focused their attention on lower frequency bands (i.e., alpha and beta), which are traditionally considered to be closely tied to the activation of sensory (van Ede et al., 2011) and/or motor cortex (Perry et al., 2011). These studies performed statistics either in the frequency or the time-frequency domain for predefined bands of interest (i.e. from 70 to 200 Hz for gamma in Guo et al., 2012; 6–14 Hz for alpha and 12–27 Hz for beta in Pihko et al., 2014; and 4–14 Hz for theta-alpha and 18–34 Hz for beta in Kurz et al., 2015a, 2015b). Here, we performed statistics in the entire spectrum from 1 to 100 Hz without a priori assumptions. We observed suppressed evoked-related power changes in the gamma frequency band (from ~40 to ~70 Hz) in both hemispheres of children with HCP compared to TD children for latencies up to ~100 ms after the stimulus onset. Gamma ERS has been previously seen in both animal (Jones and Barth, 1997) as well as human (Bauer et al., 2006) studies during tasks that require either the activation of S1 or the activation of the lemniscal afferent pathway of the somatosensory system. Deviations of our spectrograms from previous somatosensory MEG studies are possibly due to different methodological approaches and type of stimuli used (i.e. Gross et al., 2007; Kurz et al., 2015a, 2015b; 2017; Pihko et al., 2014; Witzel et al., 2011). Aberrant gamma responses in S1 may indicate abnormalities at the cortical level, possibly in the granular layer of the cortex. Locally synchronous oscillations in the gamma band have been associated with sensory stimulation (Eckhorn et al., 1988; Franowicz and Barth, 1995; MacDonald and Barth, 1995; Singer and Gray, 1995), and seem to be generated from the synchronized activity of cell populations located primarily in the granular cell layer, the largest layer in S1. Since differences were observed in early latencies up to ~100 ms, it is plausible to reflect abnormalities in the local mounting mechanism of afferent connections from the thalamus to the granular layer of the cortex within S1. These abnormalities could be due to diminished afferent inputs, which are in turn the result of an inappropriate sensory experience during development. Gamma-suppression in the S1 was observed bilaterally with no differences between hemispheres. These findings support the notion that the interplay between the S1 cortices of the MA and LA hemispheres may be also altered highlighting the complexity of functional reorganization after an early brain injury. In summary, our TFA shows evidence of suppressed gamma-responses in both hemispheres of children with HCP for early components of SEFs. This suppressed reactivity of sensory oscillations in both hemispheres may indicate abnormalities in both low- as well as high-level sensory processing mechanisms in the brain of children with HCP.

4.4. Abnormalities in the structural integrity of the AST in children with HCP

Our functionally-guided DTI findings have shown abnormalities in the structural integrity of the AST (see Fig. 6) in line with numerous previous DTI studies (Hoon et al., 2002, 2009; Thomas et al., 2005; Trivedi et al., 2010; Rose et al., 2011; Papadelis et al., 2014; Tsao et al., 2015). However, in all previous studies the AST were exclusively defined based on anatomically-defined ROI ignoring possible displacements of the functionally-relevant regions to adjacent areas due to neuroplasticity. This was indeed the case in half of our patients in whom the S1 was shifted to the pre-central gyrus for at least one digit. This type of neuroplasticity was not considered in previous DTI studies where only the postcentral gyrus was considered as the cortical target region for the AST. Moreover, our approach allows the examination of specific fibers that control the somatosensory processing of individual digits of the hand, and thus the direct correlation of behaviorally-assessed sensory abnormalities with the relevant brain structures. This is particularly important for children with HCP who can exhibit notable impairments in the realization of skilled voluntary movements, such as the precision grip between the thumb and index finger, which requires precise independent finger movements (Forssberg et al., 1999; Eliasson and Gordon, 2000).

Our data showed a significant increase in the ADC for the AST of children with HCP compared to TD children. Significant increase of ADC was also observed for the MA compared to the LA hemisphere of children with HCP. The ADC measures the magnitude of (intra- and extra-cellular) water diffusion (Le Bihan et al., 1986; Neil et al., 1998) and provides valuable information about diffusivity and myelination in the central nervous system (Grant et al., 2001, Woodhams et al., 2005; Verma et al., 2008; Gerstner et al., 2010; Menze et al., 2015). Maps of ADC in children are used to characterize myelination-related early neuro-development (Snook et al., 2005; Twomey et al., 2010; McKinstry, 2011; Yoshida et al., 2013; Erus et al., 2015; Ou et al., 2015), and to identify neuro-developmental abnormalities (Barkovich, 2000; Hüppi and Dubois, 2006; Dubois et al., 2014; Guleria and Kelly, 2014). An increase in ADC values could be suggestive of increased extracellular water content due to gliosis and microscopic cystic changes (Trivedi et al., 2010; Rai et al., 2013). This finding was accompanied by a significant increase in the RD for the children with HCP compared to TD children. Previous studies have shown that increased RD may indicate disorganized, demyelinated, dysmyelinated, and/or poorly myelinated axons (Song et al., 2002, 2005; Nair et al., 2005). Surprisingly, it was not the ADC or the RD that were positively correlated with the sensory measures, but the mean AD in the MA hemisphere of children with HCP. Increased AD has been associated with axonal injury or damage that causes a decrease in axonal density or caliber, finally resulting in an increase in the extra-axonal space allowing water molecules to move faster (Song et al., 2005; Sun et al., 2008; Kumar et al., 2010; Della Nave et al., 2011). Thus, the degree of AST axonal injury or damage in the MA hemisphere of children with hemiplegia is associated with the severity of their sensory deficits in the contralateral MA hand. Taken together, our DTI findings indicate structural abnormalities in the integrity of the AST that control the sensory function of hand digits in the MA hemisphere.

4.5. Functional abnormalities in S1 are related to structural damage of the AST

Our correlation findings between the MEG and MEG-defined PDT data support our hypothesis that functional abnormalities in the S1 of the MA hemisphere of children with HCP are the result of axonal injury or damage to the corresponding AST. The latency of the M50 component in the SEFs was positively correlated with the AD of the AST in the MA hemisphere for all three digits. This finding may be explained by the long deviations that the AST take to overcome periventricular lesions in the MA hemisphere of some of our patients having large lesions (lesion size = 3) in their MRIs (HCP3, HCP6, and HCP9). In these patients, a profound delay in the latency of M50 was observed for the MA compared to the LA hemisphere. This is in agreement with our previous MEG study (Papadelis et al., 2012) in which we also observed a profound difference in the latency of the first cortical response (N20) elicited after the electrical stimulation of median nerve between the LA and the MA hemisphere in one adult patient with HCP due to a large unilateral periventricular lesion (see Fig. 8 in Papadelis et al., 2012). Longer and/or damaged AST may indeed alter the conduction velocity of the fibers resulting in delayed cortical responses at the S1 (Purves et al., 2001; Papadelis et al., 2012). Nevertheless, statistical analysis did not reveal significant differences in the latency of M50 between the two hemispheres in the children with HCP as in previous MEG studies (i.e. Nevalainen et al., 2012). This controversy in our findings is potentially due to the inhomogeneity of our cohort, which included both patients with large cortical as well as small subcortical lesions. Statistical analysis further showed a positive correlation between the M50 amplitude and the ADC and RD, as well as a negative correlation between the relative power change in the gamma frequency and the AD of the AST for the MA hemisphere. These findings indicate pronounced changes in the excitation-inhibition balance possibly due to structural alterations in the integrity of the AST. More particularly, gamma-band oscillations, which were significantly suppressed in both hemispheres of our patients, crucially depend on negative feedback inhibition of pyramidal cells by GABAergic interactions (Sohal et al., 2009), as well as on glutamate receptor-mediated feedforward excitatory inputs (Traub et al., 2004). Two main lines of evidence suggest that this balance was impaired in our patients with HCP as indicated by the high incidence of epilepsy (Kwong et al., 1998) as well as Positron Emission Tomography data from HCP showing altered expression of GABA receptors (Lee et al., 2007; Park et al., 2013).

4.6. Study limitations

Our study examines a group of patients with HCP that have variable etiological backgrounds, different clinical histories (i.e. preterm vs. term birth), and different types of brain lesions (i.e. periventricular white matter injury vs. lesions involving the cortex). Both developing children (2–12 years old) as well as adolescences (12–18 years old) were included in the study. Thus, the functional and structural changes observed in our cohort of patients may not apply to all underlying pathologies of HCP. For example, it is possible that the abnormal functional processing and sensory deficits in the children with cortical damage in our patients are not necessarily due to damage to the AST alone but also due to damage to the cortex itself. Moreover, our patients may present different types of motor reorganization (e.g. ipsilateral, bilateral, or normal contralateral representation of the affected upper extremity), which may also affect at least partly aspects of the cortical sensory representation and function.

The morphologies of SEFs were striking different between the LA and the MA hemispheres in children with HCP, and in most cases between the children with HCP and the TD children. The most prominent morphological differences were observed for the three children with large unilateral lesions. These prominent differences between the two hemispheres in HCP children indicate that there are possible functional deficits also in the secondary processing areas of the somatosensory cortex, as well as deficits in the functional connectivity among the primary and secondary somatosensory areas. However, these observations are descriptive in nature. Further research is required to explore the later components of SEFs and their functional connectivity to the initial entry of information to S1.

In the current study, we used a partial coverage MEG system that is unable to capture activations located in brain regions that are not covered by the array. Such activations may affect the amplitude of MNE maximas at locations inside the coverage area. However, it is quite unlikely that the first somatosensory response would be generated by multiple underlying generators, which are simultaneously active and located at distant locations that fall apart few centimeters. For the forward model, we used a whole head BEM. Our motivation to use realistic head models was justified by our cohort, which also included patients with large cortical lesions. Previous studies have shown that BEM is superior to spherical head-models, provided that individually-defined inner skull and scalp meshes are used (Henson et al., 2009). However, the benefits/pitfalls of using a whole brain BEM with a partial coverage MEG sensor array is not well-examined. Our group has used BEM in a series of previous studies with the BabySQUID system (Papadelis et al., 2013, 2014; Khan et al., 2014; Hunold et al., 2014), but the head model selection and its effect on localization findings were not examined. Previous researchers used different head models for partial coverage systems. For example, Ahlfors et al. (1992) used a partial array to measure visual activity and computed the MNE using a single sphere with a 60 mm radius that was optimized for the curvature of the occipital cortex. Here, the selection of the head model is a tradeoff between an appropriate model for patients with large cortical lesions and a model that is not ideal for partial coverage arrays. Although magnetic fields are not distorted by the inhomogeneous tissue conductivity and the volume conduction effect, inappropriate head models may alter the localization findings. However, this alteration has been shown to be negligible (< 1 mm) for superficial sources in previous phantom studies (Leahy et al., 1998; Papadelis et al., 2009). Future research is required to define the appropriateness of the head model selection for partial coverage MEG systems, such as the BabySQUID.

5. Conclusions

We associate for the first time measures of bilateral altered functional cortical organization in S1 of children with HCP with deficient structural integrity of the AST. We further correlate the degree of the AST injury or damage with the severity of sensory deficits in the contralateral hand. Our findings indicate bilateral maladaptive functional changes in the S1 of children with HCP, which were expressed as suppressed gamma responses– possibly due to changes in the excitation-inhibition balance of the pyramidal neurons— and alterations in the cortical body representation. These functional changes at the cortical level are correlated to the severity of axonal damage in the AST projecting to the MA hemisphere. Our findings support the notion that the functional organization of S1 is modulated by the long-lasting experience of decreased or altered sensory input, as a result of diminished thalamocortical projections (Merzenich et al., 1984; Flor et al., 1995). They further suggest that a significant contributor to the upper-limb motor impairments in children with HCP is an abnormal somatosensory system as a result of axonal injury or damage to the AST. Although functional changes in the S1 were observed bilaterally in our cohort of patients, abnormalities in the structural integrity of the AST were mostly unilateral in the hemisphere contralateral to the paretic hand. The data of the current study are not sufficient to clearly disentangle all aspects of this brain reorganization mechanism. However, they allow us to speculate that bilateral functional changes in the S1 of the brain of HCP are due to transferred abnormal sensory information between the two hemispheres possibly via the callosal connections of S1 (Manzoni et al., 1989). This is in line with the most updated view of S1 as an integrator of somatosensory inputs from both sides of the body rather than a simple relay of unilateral sensory information (Tamè et al., 2015, 2016). Despite the fact that our study is limited by the inhomogeneous pathologies causing HCP in our cohort, it provides detailed insights into the neurophysiological mechanisms that are responsible for the uncharacteristic somatosensory processing observed in these children.

Acknowledgements

This work was supported by internal funding from the Fetal-Neonatal Neuroimaging & Developmental Science Center, and the Division of Newborn Medicine at Boston Children's Hospital. We gratefully thank Chiran Doshi and Banu Ahtam for their help with the MEG and MRI recordings, Eleonora Tamilia for her help with PDT data analysis, and Michel Al Hilani for his help with MEG data analysis. The recruitment of children with HCP was performed by B.S. and C.P. through the CP Clinic at Boston Children's Hospital. MEG and MRI data were collected by C.P., MEG data analysis was performed by E.E.B. and M.R., TFA was performed by L.S., PDT was performed by M.R. and supervised by C.P. and L.Z., while the manuscript was prepared by all authors.

References

Ahlfors, S.P., Ilmoniemi, R.J., Hamalainen, M.S., 1992. Estimates of visually evoked cortical currents. Electroencephalogr. Clin. Neurol. 82, 225–236.
Aranibar, A., Pfurtscheller, G., 1978. On and off effects in the background EEG activity during one-second photic stimulation. Electroencephalogr. Clin. Neurophysiol. 44 (3), 307–316.
Auld, M.L., Boyd, R.N., Moseley, G.L., Ware, R.S., Johnston, L.M., 2012. Impact of tactile dysfunction on upper-limb motor performance in children with unilateral cerebral palsy. Arch. Phys. Med. Rehabil. 93 (4), 696–702.
Baillet, S., Mosher, J.C., Leahy, R.M., 2001. Electromagnetic brain mapping. IEEE Signal Process. Mag. 18 (6), 14–30.

Barkovich, A.J., 2000. Concepts of myelin and myelination in neuroradiology. Am. J. Neuroradiol. 21 (6), 1099–1109.
Bauer, M., Oostenveld, R., Peeters, M., Fries, P., 2006. Tactile spatial attention enhances gamma-band activity in somatosensory cortex and reduces low-frequency activity in parieto-occipital areas. J. Neurosci. 26 (2), 490–501.
Behrens, T.E., Berg, H.J., Jbabdi, S., Rushworth, M.F., Woolrich, M.W., 2007. Probabilistic diffusion tractography with multiple fibre orientations: what can we gain? NeuroImage 34 (1), 144–155.
Burton, H., Dixit, S., Litkowski, P., Wingert, J.R., 2009. Functional connectivity for somatosensory and motor cortex in spastic diplegia. Somatosens. Mot. Res. 26 (4), 90–104.
Candia, V., Wienbruch, C., Elbert, T., Rockstroh, B., Ray, W., 2003. Effective behavioral treatment of focal hand dystonia in musicians alters somatosensory cortical organization. Proc. Natl. Acad. Sci. U. S. A. 100 (13), 7942–7946.
Cascio, C.J., 2010. Somatosensory processing in neurodevelopmental disorders. J. Neurodev. Disord. 2 (2), 62–69.
Ciccarelli, O., Behrens, T.E., Altmann, D.R., Orrell, R.W., Howard, R.S., Johansen-Berg, H., Miller, D.H., Matthews, P.M., Thompson, A.J., 2006. Probabilistic diffusion tractography: a potential tool to assess the rate of disease progression in amyotrophic lateral sclerosis. Brain 129 (Pt 7), 1859–1871.
Coq, J.O., Strata, F., Russier, M., Safadi, F.F., Merzenich, M.M., Byl, N.N., Barbe, M.F., 2008. Impact of neonatal asphyxia and hind limb immobilization on musculoskeletal tissues and S1 map organization: implications for cerebral palsy. Exp. Neurol. 210 (1), 95–108.
Crone, N.E., Miglioretti, D.L., Gordon, B., Lesser, R.P., 1998. Functional mapping of human sensorimotor cortex with electrocorticographic spectral analysis. II. Event-related synchronization in the gamma band. Brain 121, 2301–2315.
Dale, A.M., Fischl, B., Sereno, M.I., 1999. Cortical surface-based analysis. I. Segmentation and surface reconstruction. NeuroImage 9 (2), 179–194.
Della Nave, R., Ginestroni, A., Diciotti, S., Salvatore, E., Soricelli, A., Mascalchi, M., 2011. Axial diffusivity is increased in the degenerating superior cerebellar peduncles of Friedreich's ataxia. Neuroradiology 53 (5), 367–372.
Dubois, J., Dehaene-Lambertz, G., Kulikova, S., Poupon, C., Huppi, P.S., Hertz-Pannier, L., 2014. The early development of brain white matter: a review of imaging studies in fetuses, newborns and infants. Neuroscience 12 (276), 48–71.
Eckhorn, R., Bauer, R., Jordon, W., Brosch, M., Kruse, W., Munk, M., Reitboeck, H.J., 1988. Coherent oscillations: a mechanism of feature linking in the visual cortex? Biol. Cybern. 60, 121–130.
Eliasson, A.C., Gordon, A.M., 2000. Impaired force coordination during object release in children with hemiplegic cerebral palsy. Dev. Med. Child Neurol. 42, 228–234.
Eliasson, A.C., Krumlinde-Sundholm, L., Rösblad, B., Beckung, E., Arner, M., Ohrvall, A.M., Rosenbaum, P., 2006. The manual ability classification system (MACS) for children with cerebral palsy: scale development and evidence of validity and reliability. Dev. Med. Child Neurol. 48 (7), 549–554.
Erus, G., Battapady, H., Satterthwaite, T.D., Hakonarson, H., Gur, R.E., Davatzikos, C., Gur, R.C., 2015. Imaging patterns of brain development and their relationship to cognition. Cereb. Cortex 25 (6), 1676–1684.
Fischl, B., 2012. FreeSurfer. NeuroImage 62 (2), 774–781.
Flor, H., Elbert, T., Knecht, S., Wienbruch, C., Pantev, C., Birbaumer, N., Larbig, W., Taub, E., 1995. Phantom-limb pain as a perceptual correlate of cortical reorganization following arm amputation. Nature 375 (6531), 482–484.
Forssberg, H., Eliasson, A.C., Redon-Zouitenn, C., Mercuri, E., Dubowitz, L., 1999. Impaired grip-lift synergy in children with unilateral brain lesions. Brain 122 (Pt 6), 1157–1168.
Franowicz, M.N., Barth, D.S., 1995. Comparison of evoked potentials and high-frequency (gamma-band) oscillating potentials in rat auditory cortex. J. Neurophysiol. 74 (1), 96–112.
Fukuda, M., Nishida, M., Juhász, C., Muzik, O., Sood, S., Chugani, H.T., Asano, E., 2008. Short-latency median-nerve somatosensory-evoked potentials and induced gamma-oscillations in humans. Brain 131 (Pt 7), 1793–1805.
Gerstner, E.R., Chen, P.J., Wen, P.Y., Jain, R.K., Batchelor, T.T., Sorensen, G., 2010. Infiltrative patterns of glioblastoma spread detected via diffusion MRI after treatment with cediranib. Neuro-Oncology 12 (5), 466–472.
Gondo, K., Kira, H., Tokunaga, Y., Harashima, C., Tobimatsu, S., Yamamoto, T., Hara, T., 2000. Reorganization of the primary somatosensory area in epilepsy associated with focal cortical dysplasia. Dev. Med. Child Neurol. 42 (12), 839–842.
Gramfort, A., Papadopoulo, T., Olivi, E., Clerc, M., 2010. OpenMEEG: opensource software for quasistatic bioelectromagnetics. Biomed. Eng. Online 9, 45.
Grant, P.E., He, J., Halpern, E.F., Wu, O., Schaefer, P.W., Schwamm, L.H., Budzik, R.F., Sorensen, A.G., Koroshetz, W.J., Gonzalez, R.G., 2001. Frequency and clinical context of decreased apparent diffusion coefficient reversal in the human brain. Radiology 221 (1), 43–50.
Gross, J., Schnitzler, A., Timmermann, L., Ploner, M., 2007. Gamma oscillations in human primary somatosensory cortex reflect pain perception. PLoS Biol. 5 (5), e133.
Guleria, S., Kelly, T.G., 2014. Myelin, myelination, and corresponding magnetic resonance imaging changes. Radiol. Clin. N. Am. 52 (2), 227–239.
Guo, X., Xiang, J., Mun-Bryce, S., Bryce, M., Huang, S., Huo, X., Wang, Y., Rose, D., Degrauw, T., Gartner, K., et al., 2012. Aberrant high-gamma oscillations in the somatosensory cortex of children with cerebral palsy: a MEG study. Brain Dev. 34 (7), 576–583.
Guye, M., Parker, G.J., Symms, M., Boulby, P., Wheeler-Kingshott, C.A., Salek-Haddadi, A., Barker, G.J., Duncan, J.S., 2003. Combined functional MRI and tractography to demonstrate the connectivity of the human primary motor cortex in vivo. NeuroImage 19 (4), 1349–1360.
Hämäläinen, M.S., Ilmoniemi, R.J., 1984. Interpreting Measured Magnetic Fields of the Brain: Estimates of Current Distributions. Tech. Rep. TKK-F-A559. Helsinki University of Technology, Espoo.
Hari, R., Joutsiniemi, S.L., Sarvas, J., 1988. Spatial resolution of neuromagnetic records: theoretical calculations in a spherical model. Electroencephalogr. Clin. Neurophysiol. 71, 64–72.
Hari, R., Karhu, J., Hämäläinen, M., Knuutila, J., Salonen, O., Sams, M., Vilkman, V., 1993. Functional organization of the human first and second somatosensory cortices: a neuromagnetic study. Eur. J. Neurosci. 5 (6), 724–734.
Hauk, O., Wakeman, D.G., Henson, R., 2011. Comparison of noise-normalized minimum norm estimates for MEG analysis using multiple resolution metrics. NeuroImage 54, 1966–1974.
Henson, R.N., Mattout, J., Phillips, C., Friston, K.J., 2009. Selecting forward models for MEG source-reconstruction using model-evidence. NeuroImage 46, 168–176.
Hlustík, P., Solodkin, A., Gullapalli, R.P., Noll, D.C., Small, S.L., 2001. Somatotopy in human primary motor and somatosensory hand representations revisited. Cereb. Cortex 11 (4), 312–321.
Hoon Jr., A.H., Lawrie Jr., W.T., Melhem, E.R., Reinhardt, E.M., Van Zijl, P.C., Solaiyappan, M., Jiang, H., Johnston, M.V., Mori, S., 2002. Diffusion tensor imaging of periventricular leukomalacia shows affected sensory cortex white matter pathways. Neurology 59 (5), 752–756.
Hoon Jr., A.H., Stashinko, E.E., Nagae, L.M., Lin, D.D., Keller, J., Bastian, A., Campbell, M.L., Levey, E., Mori, S., Johnston, M.V., 2009. Sensory and motor deficits in children with cerebral palsy born preterm correlate with diffusion tensor imaging abnormalities in thalamocortical pathways. Dev. Med. Child Neurol. 51 (9), 697–704.
Hunold, A., Haueisen, J., Ahtam, B., Doshi, C., Harini, C., Camposano, S., Warfield, S.K., Grant, P.E., Okada, Y., Papadelis, C., 2014. Localization of the epileptogenic foci in tuberous sclerosis complex: a pediatric case report. Front. Hum. Neurosci. 8, 175.
Hunter, J., Mackin, E., Callahan, A., 1995. Rehabilitation for the Hand: Surgery, and Therapy. Mosby, St. Louis (MO).
Hüppi, P.S., Dubois, J., 2006. Diffusion tensor imaging of brain development. Semin. Fetal Neonatal Med. 11 (6), 489–497.
Jones, M.S., Barth, D.S., 1997. Sensory-evoked high-frequency (gamma-band) oscillating potentials in somatosensory cortex of the unanesthetized rat. Brain Res. 768 (1–2), 167–176.
Jung, P., Baumgärtner, U., Magerl, W., Treede, R.D., 2008. Hemispheric asymmetry of hand representation in human primary somatosensory cortex and handedness. Clin. Neurophysiol. 119 (11), 2579–2586.
Keizer, D., Fael, D., Wierda, J.M., van Wijhe, M., 2008. Quantitative sensory testing with Von Frey monofilaments in patients with allodynia: what are we quantifying? Clin. J. Pain 24 (5), 463–466.
Khan, S., Lefèvre, J., Baillet, S., Michmizos, K.P., Ganesan, S., Kitzbichler, M.G., Zetino, M., Hämäläinen, M.S., Papadelis, C., Kenet, T., 2014. Encoding cortical dynamics in sparse features. Front. Hum. Neurosci. 8, 338.
Kinnucan, E., Van Heest, A., Tomhave, W., 2010. Correlation of motor function and stereognosis impairment in upper limb cerebral palsy. J. Hand. Surg. [Am.] 35 (8), 1317–1322.
Kumar, A., Sundaram, S.K., Sivaswamy, L., Behen, M.E., Makki, M.I., Ager, J., Janisse, J., Chugani, H.T., Chugani, D.C., 2010. Alterations in frontal lobe tracts and corpus callosum in young children with autism spectrum disorder. Cereb. Cortex 20 (9), 2103–2113.
Kurz, M.J., Wilson, T.W., 2011. Neuromagnetic activity in the somatosensory cortices of children with cerebral palsy. Neurosci. Lett. 490 (1), 1–5.
Kurz, M.J., Heinrichs-Graham, E., Arpin, D.J., Becker, K.M., Wilson, T.W., 2014. Aberrant synchrony in the somatosensory cortices predicts motor performance errors in children with cerebral palsy. J. Neurophysiol. 111, 573–579.
Kurz, M.J., Becker, K.M., Heinrichs-Graham, E., Wilson, T.W., 2015a. Children with cerebral palsy have uncharacteristic somatosensory cortical oscillations after stimulation of the hand mechanoreceptors. Neuroscience 305, 67–75.
Kurz, M.J., Heinrichs-Graham, E., Becker, K.M., Wilson, T.W., 2015b. The magnitude of the somatosensory cortical activity is related to the mobility and strength impairments seen in children with cerebral palsy. J. Neurophysiol. 113 (9), 3143–3150.
Kwong, K.L., Wong, S.N., So, K.T., 1998. Epilepsy in children with cerebral palsy. Pediatr. Neurol. 19 (1), 31–36.
Le Bihan, D., Breton, E., Lallemand, D., Grenier, P., Cabanis, E., Laval-Jeantet, M., 1986. MR imaging of intravoxel incoherent motions: application to diffusion and perfusion in neurologic disorders. Radiology 161 (2), 401–407.
Leahy, R.M., Mosher, J.C., Spencer, M.E., Huang, M.X., Lewine, J.D., 1998. A study of dipole localization accuracy for MEG and EEG using a human skull phantom. Electroencephalogr. Clin. Neurophysiol. 107, 159–173.
Lee Dellon, A., 1997. Somatosensory Testing and Rehabilitation. AOTA, Bethesda (MD).
Lee, J.D., Park, H.J., Park, E.S., Kim, D.G., Rha, D.W., Kim, E.Y., Kim, D.I., Kim, J.J., Yun, M., Ryu, Y.H., Lee, J., Jeong, J.M., Lee, D.S., Lee, M.C., Park, C.I., 2007. Assessment of regional GABA(a) receptor binding using 18F-fluoroflumazenil positron emission tomography in spastic type cerebral palsy. NeuroImage 34 (1), 19–25.
Lesný, I., Stehlík, A., Tomásek, J., Tománková, A., Havlícek, I., 1993. Sensory disorders in cerebral palsy: two-point discrimination. Dev. Med. Child Neurol. 35 (5), 402–405.
Lin, F.H., Witzel, T., Ahlfors, S.P., Stufflebeam, S.M., Belliveau, J.W., Hämäläinen, M.S., 2006. Assessing and improving the spatial accuracy in MEG source localization by depth-weighted minimum-norm estimates. NeuroImage 31, 160–171.
Liu, A.K., Dale, A.M., Belliveau, J.W., 2002. Monte Carlo simulation studies of EEG and MEG localization accuracy. Hum. Brain Mapp. 16, 47–62.
MacDonald, K.D., Barth, D.S., 1995. High frequency (gamma-band) oscillating potentials in rat somatosensory and auditory cortex. Brain Res. 694 (1–2), 1–12.
Maitre, N.L., Barnett, Z.P., Key, A.P., 2012. Novel assessment of cortical response to somatosensory stimuli in children with hemiparetic cerebral palsy. J. Child Neurol. 27 (10), 1276–1283.
Maldjian, J.A., Gottschalk, A., Patel, R.S., Detre, J.A., Alsop, D.C., 1999. The sensory

somatotopic map of the human hand demonstrated at 4 tesla. NeuroImage 10 (1), 55–62.
Manzoni, T., Barbaresi, P., Conti, F., Fabri, M., 1989. The callosal connections of the primary somatosensory cortex and the neural bases of midline fusion. Exp. Brain Res. 76 (2), 251–266.
Maris, E., Oostenveld, R., 2007. Nonparametric statistical testing of EEG- and MEG-data. J. Neurosci. Methods 164 (1), 177–190.
Mauguière, F., Merlet, I., Forss, N., Vanni, S., Jousmäki, V., Adeleine, P., Hari, R., 1997. Activation of a distributed somatosensory cortical network in the human brain. A dipole modelling study of magnetic fields evoked by median nerve stimulation. Part I: location and activation timing of SEF sources. Electroencephalogr. Clin. Neurophysiol. 104 (4), 281–289.
McKinstry, R.C., 2011. Advances in pediatric diffusion tensor imaging. Pediatr. Radiol. 41, 137–138.
Menze, B.H., Jakab, A., Bauer, S., Kalpathy-Cramer, J., Farahani, K., Kirby, J., Burren, Y., Porz, N., Slotboom, J., Wiest, R., et al., 2015. The multimodal brain tumor image segmentation benchmark (BRATS). IEEE Trans. Med. Imaging 34 (10), 1993–2024.
Merzenich, M.M., Nelson, R.J., Stryker, M.P., Cynader, M.S., Schoppmann, A., Zook, J.M., 1984. Somatosensory cortical map changes following digit amputation in adult monkeys. J. Comp. Neurol. 224 (4), 591–605.
Nair, G., Tanahashi, Y., Low, H.P., Billings-Gagliardi, S., Schwartz, W.J., Duong, T.Q., 2005. Myelination and long diffusion times alter diffusion-tensor-imaging contrast in myelin-deficient shiverer mice. NeuroImage 28 (1), 165–174.
Nakamura, A., Yamada, T., Goto, A., Kato, T., Ito, K., Abe, Y., Kachi, T., Kakigi, R., 1998. Somatosensory homunculus as drawn by MEG. NeuroImage 7 (4 Pt 1), 377–386.
Neil, J.J., Shiran, S.I., McKinstry, R.C., Schefft, G.L., Snyder, A.Z., Almli, C.R., Akbudak, E., Aronovitz, J.A., Miller, J.P., Lee, B.C., et al., 1998. Normal brain in human newborns: apparent diffusion coefficient and diffusion anisotropy measured by using diffusion tensor MR imaging. Radiology 209 (1), 57–66.
Nevalainen, P., Pihko, E., Mäenpää, H., Valanne, L., Nummenmaa, L., Lauronen, L., 2012. Bilateral alterations in somatosensory cortical processing in hemiplegic cerebral palsy. Dev. Med. Child Neurol. 54 (4), 361–367.
Oishi, K., Faria, A., van Zijl, P.C.M., Mori, S., 2011. MRI Atlas of Human White Matter. Elsevier, Amsterdam (DE).
Okada, Y., Pratt, K., Atwood, C., Mascarenas, A., Reineman, R., Nurminen, J., Paulson, D., 2006. BabySQUID: a mobile, high-resolution multichannel magnetoencephalography system for neonatal brain assessment. Rev. Sci. Instrum. 77, 2.
Oouchida, Y., Sudo, T., Inamura, T., Tanaka, N., Ohki, Y., Izumi, S., 2016. Maladaptive change of body representation in the brain after damage to central or peripheral nervous system. Neurosci. Res. 104, 38–43.
Ou, Y., Gollub, R.L., Retzepi, K., Reynolds, N., Pienaar, R., Pieper, S., Murphy, S.N., Grant, P.E., Zollei, L., 2015. Brain extraction in pediatric ADC maps, toward characterizing neuro-development in multi-platform and multi-institution clinical images. NeuroImage 15 (122), 246–261.
Palisano, R., Rosenbaum, P., Walter, S., Russell, D., Wood, E., Galuppi, B., 1997. Development and reliability of a system to classify gross motor function in children with cerebral palsy. Dev. Med. Child Neurol. 39 (4), 214–223.
Papadelis, C., Poghosyan, V., Fenwick, P.B., Ioannides, A.A., 2009. MEG's ability to localise accurately weak transient neural sources. Clin. Neurophysiol. 120 (11), 1958–1970.
Papadelis, C., Eickhoff, S.B., Zilles, K., Ioannides, A.A., 2011. BA3b and BA1 activate in a serial fashion after median nerve stimulation: direct evidence from combining source analysis of evoked fields and cytoarchitectonic probabilistic maps. NeuroImage 54 (1), 60–73.
Papadelis, C., Leonardelli, E., Staudt, M., Braun, C., 2012. Can magnetoencephalography track the afferent information flow along white matter thalamo-cortical fibers? NeuroImage 60 (2), 1092–1105.
Papadelis, C., Harini, C., Ahtam, B., Doshi, C., Grant, E., Okada, Y., 2013. Current and emerging potential for magnetoencephalography in pediatric epilepsy. J. Pedriatr. Epilepsy 2, 73–85.
Papadelis, C., Ahtam, B., Nazarova, M., Nimec, D., Snyder, B., Grant, P.E., Okada, Y., 2014. Cortical somatosensory reorganization in children with spastic cerebral palsy: a multimodal neuroimaging study. Front. Hum. Neurosci. 12 (8), 725.
Papadelis, C., Arfeller, C., Erla, S., Nollo, G., Cattaneo, L., Braun, C., 2016. Inferior frontal gyrus links visual and motor cortices during a visuomotor precision grip force task. Brain Res. 1650, 252–266.
Park, H.J., Kim, C.H., Park, E.S., Park, B., Oh, S.R., Oh, M.K., Park, C.I., Lee, J.D., 2013. Increased GABA-A receptor binding and reduced connectivity at the motor cortex in children with hemiplegic cerebral palsy: a multimodal investigation using 18F-fluoroflumazenil PET, immunohistochemistry, and MR imaging. J. Nucl. Med. 54 (8), 1263–1269.
Perry, A., Stein, L., Bentin, S., 2011. Motor and attentional mechanisms involved in social interaction–evidence from mu and alpha EEG suppression. NeuroImage 58 (3), 895–904.
Pihko, E., Nevalainen, P., Vaalto, S., Laaksonen, K., Mäenpää, H., Valanne, L., Lauronen, 2014. Reactivity of sensorimotor oscillations is altered in children with hemiplegic cerebral palsy: a magnetoencephalographic study. Hum. Brain Mapp. 35 (8), 4105–4117.
Pleger, B., Foerster, A.F., Ragert, P., Dinse, H.R., Schwenkreis, P., Malin, J.P., Nicolas, V., Tegenthoff, M., 2003. Functional imaging of perceptual learning in human primary and secondary somatosensory cortex. Neuron 40, 643–653.
Porter, L.L., 1997. Morphological characterization of a cortico-cortical relay in the cat sensorimotor cortex. Cereb. Cortex 7 (2), 100–109.
Purves, D., Augustine, G.J., Fitzpatrick, D., Katz, L.C., LaMantia, A., McNamara, J.O., Williams, S.M., 2001. Neuroscience, 2nd edition. Sinauer Associates, Sunderland (MA).
Rai, Y., Chaturvedi, S., Paliwal, V.K., Goyal, P., Chourasia, A., Singh Rathore, R.K., Yadav, A., Pandey, C.M., Lalla, R.S., Garg, R.K., et al., 2013. DTI correlates of cognition in term children with spastic diplegic cerebral palsy. Eur. J. Paediatr. Neurol. 17 (3), 294–301.
Rao, S.M., Binder, J.R., Bandettini, P.A., Hammeke, T.A., Yetkin, F.Z., Jesmanowicz, A., Lisk, L.M., Morris, G.L., Mueller, M.W., Estkowski, L.D., et al., 1993. Functional magnetic resonance imaging of complex human movements. Neurology 43, 2311–2318.
Reid, L.B., Cunnington, R., Boyd, R.N., Rose, S.E., 2016. Correction: surface-based fMRI-driven diffusion tractography in the presence of significant brain pathology: a study linking structure and function in cerebral palsy. PLoS One 11 (8), e0162271.
Riquelme, I., Montoya, P., 2010. Developmental changes in somatosensory processing in cerebral palsy and healthy individuals. Clin. Neurophysiol. 121 (8), 1314–1320.
Rose, S., Guzzetta, A., Pannek, K., Boyd, R., 2011. MRI structural connectivity, disruption of primary sensorimotor pathways, and hand function in cerebral palsy. Brain Connect. 1 (4), 309–316.
Rosenbaum, P., Paneth, N., Leviton, A., Goldstein, M., Bax, M., Damiano, D., Dan, B., Jacobsson, B., 2007. A report: the definition and classification of cerebral palsy. Dev. Med. Child Neurol. 49 (Suppl. 109), 8–14.
Sanger, T.D., Kukke, S.N., 2007. Abnormalities of tactile sensory function in children with dystonic and diplegic cerebral palsy. J. Child Neurol. 22 (3), 289–293.
Singer, W., Gray, C.M., 1995. Visual feature integration and the temporal correlation hypothesis. Annu. Rev. Neurosci. 18, 555–586.
Snook, L., Paulson, L.A., Roy, D., Phillips, L., Beaulieu, C., 2005. Diffusion tensor imaging of neurodevelopment in children and young adults. NeuroImage 26 (4), 1164–1173.
Soares, J.M., Marques, P., Alves, V., Sousa, N., 2013. A hitchhiker's guide to diffusion tensor imaging. Front. Neurosci. 7, 31.
Soechting, J.F., Flanders, M., 2008. Sensorimotor control of contact force. Curr. Opin. Neurobiol. 18 (6), 565–572.
Sohal, V.S., Zhang, F., Yizhar, O., Deisseroth, K., 2009. Parvalbumin neurons and gamma rhythms enhance cortical circuit performance. Nature 459 (7247), 698–702.
Song, S.K., Sun, S.W., Ramsbottom, M.J., Chang, C., Russell, J., Cross, A.H., 2002. Dysmyelination revealed through MRI as increased radial (but unchanged axial) diffusion of water. NeuroImage 17 (3), 1429–1436.
Song, S.K., Yoshino, J., Le, T.Q., Lin, S.J., Sun, S.W., Cross, A.H., Armstrong, R.C., 2005. Demyelination increases radial diffusivity in corpus callosum of mouse brain. NeuroImage 26 (1), 132–140.
Sterr, A., Müller, M.M., Elbert, T., Rockstroh, B., Pantev, C., Taub, E., 1998. Perceptual correlates of changes in cortical representation of fingers in blind multifinger braille readers. J. Neurosci. 18 (11), 4417–4423.
Sun, S.Q., Liang, H.F., Cross, A.H., Song, S.K., 2008. Evolving Wallerian degeneration after transient retinal ischemia in mice characterized by diffusion tensor imaging. NeuroImage 1 (40), 1–10.
Tadel, F., Baillet, S., Mosher, J.C., Pantazis, D., Leahy, R.M., 2011. Brainstorm: a user-friendly application for MEG/EEG analysis. Comput. Intell. Neurosci. 879716.
Tamè, L., Pavani, F., Papadelis, C., Farnè, A., Braun, C., 2015. Early integration of bilateral touch in the primary somatosensory cortex. Hum. Brain Mapp. 36 (4), 1506–1523.
Tamè, L., Braun, C., Holmes, N.P., Farnè, A., Pavani, F., 2016. Bilateral representations of touch in the primary somatosensory cortex. Cogn. Neuropsychol. 33 (1–2), 48–66.
Tecchio, F., Babiloni, C., Zappasodi, F., Vecchio, F., Pizzella, V., Romani, G.L., Rossini, P.M., 2003. Gamma synchronization in human primary somatosensory cortex as revealed by somatosensory evoked neuromagnetic fields. Brain Res. 986 (1–2), 63–70.
Tecchio, F., Zappasodi, F., Porcaro, C., Barbati, G., Assenza, G., Salustri, C., Rossini, P.M., 2008. High-gamma band activity of primary hand cortical areas: a sensorimotor feedback efficiency index. NeuroImage 40 (1), 256–264.
Teflioudi, E.P., Zafeiriou, D.I., Vargiami, E., Kontopoulos, E., Tsikoulas, I., 2011. Somatosensory evoked potentials in children with bilateral spastic cerebral palsy. Pediatr. Neurol. 44 (3), 177–182.
Thomas, B., Eyssen, M., Peeters, R., Molenaers, G., Van Hecke, P., De Cock, P., Sunaert, S., 2005. Quantitative diffusion tensor imaging in cerebral palsy due to periventricular white matter injury. Brain 128 (Pt 11), 2562–2577.
Traub, R.D., Bibbig, A., LeBeau, F.E., Buhl, E.H., Whittington, M.A., 2004. Cellular mechanisms of neuronal population oscillations in the hippocampus in vitro. Annu. Rev. Neurosci. 27, 247–278.
Trivedi, R., Agarwal, S., Shah, V., Goyel, P., Paliwal, V.K., Rathore, R.K., Gupta, R.K., 2010. Correlation of quantitative sensorimotor tractography with clinical grade of cerebral palsy. Neuroradiology 52 (8), 759–765.
Tsao, H., Pannek, K., Boyd, R.N., Rose, S.E., 2015. Changes in the integrity of thalamocortical connections are associated with sensorimotor deficits in children with congenital hemiplegia. Brain Struct. Funct. 220 (1), 307–318.
Twomey, E., Twomey, A., Ryan, S., Murphy, J., Donoghue, V.B., 2010. MR imaging of term infants with hypoxic-ischaemic encephalopathy as a predictor of neurodevelopmental outcome and late MRI appearances. Pediatr. Radiol. 40 (9), 1526–1535.
van Ede, F., de Lange, F., Jensen, O., Maris, E., 2011. Orienting attention to an upcoming tactile event involves a spatially and temporally specific modulation of sensorimotor alpha- and beta-band oscillations. J. Neurosci. 31 (6), 2016–2024.
Verma, R., Zacharaki, E.I., Ou, Y., Cai, H., Chawla, S., Lee, S.K., Melhem, E.R., Wolf, R., Davatzikos, C., 2008. Multiparametric tissue characterization of brain neoplasms and their recurrence using pattern classification of MR images. Acad. Radiol. 15 (8), 966–977.
Wilke, M., Staudt, M., 2009. Does damage to somatosensory circuits underlie motor impairment in cerebral palsy? Dev. Med. Child Neurol. 51 (9), 686–687.
Wingert, J.R., Burton, H., Sinclair, R.J., Brunstrom, J.E., Damiano, D.L., 2008. Tactile sensory abilities in cerebral palsy: deficits in roughness and object discrimination. Dev. Med. Child Neurol. 50 (11), 832–838.

Wingert, J.R., Sinclair, R.J., Dixit, S., Damiano, D.L., Burton, H., 2010. Somatosensory-evoked cortical activity in spastic diplegic cerebral palsy. Hum. Brain Mapp. 31 (11), 1772–1785.

Witzel, T., Napadow, V., Kettner, N.W., Vangel, M.G., Hämäläinen, M.S., Dhond, R.P., 2011. Differences in cortical response to acupressure and electroacupuncture stimuli. BMC Neurosci. 12, 73.

Woodhams, R., Matsunaga, K., Iwabuchi, K., Kan, S., Hata, H., Kuranami, M., Wantanabe, M., Hayakawa, K., 2005. Diffusion-weighted imaging of malignant breast tumors: the usefulness of apparent diffusion coefficient (ADC) value and ADC map for the detection of malignant breast tumors and evaluation of cancer extension. J. Comput. Assist. Tomogr. 29 (5), 644–649.

Woolrich, M.W., Jbabdi, S., Patenaude, B., Chappell, M., Makni, S., Behrens, T., Beckmann, C., Jenkinson, M., Smith, S.M., 2009. Bayesian analysis of neuroimaging data in FSL. NeuroImage 45 (1 Suppl), S173–86.

Yoshida, S., Oishi, K., Faria, A.V., Mori, S., 2013. Diffusion tensor imaging of normal brain development. Pediatr. Radiol. 43 (1), 15–27.